

Age and Metallicity Distribution of the Galactic Bulge from Extensive Optical and Near-IR Stellar Photometry [★]

M. Zoccali¹, A. Renzini¹, S. Ortolani², L. Greggio³, I. Saviane⁴, S. Cassisi⁵, M. Rejkuba¹, B. Barbuy⁶, R.M. Rich⁷, E. Bica⁸

¹ European Southern Observatory, Karl Schwarzschild Strasse 2, D-85748, Garching bei München, Germany; mzoccali@eso.org, arenzini@eso.org, mrejkuba@eso.org

² Università di Padova, Dipart. di Astronomia, Vicolo dell'Osservatorio 2, I-35122 Padova, Italy; ortolani@pd.astro.it

³ INAF, Osservatorio Astronomico di Padova, Padova, Italy; greggio@pd.astro.it

⁴ European Southern Observatory, Alonso de Cordova 3107, Santiago 19, Chile; isaviane@eso.org

⁵ INAF, Osservatorio Astronomico Collurania, I-64100, Teramo, Italy; cassisi@te.astro.it

⁶ Universidade de São Paulo, CP 3386, São Paulo 01060-970, Brazil; barbuy@astro.iag.usp.br

⁷ Department of Physics and Astronomy, Division of Astronomy and Astrophysics, University of California, Los Angeles, CA 90095-1562; rmr@astro.ucla.edu

⁸ Universidade Federal do Rio Grande do Sul, Dept. de Astronomia, CP 15051, Porto Alegre 91501-970, Brazil; bica@if.ufrgs.br

Received date / Accepted date

Abstract. We present a new determination of the metallicity distribution, age, and luminosity function of the Galactic bulge stellar population. By combining near-IR data from the 2MASS survey, from the SOFI imager at ESO NTT and the NICMOS camera on board HST we were able to construct color-magnitude diagrams (CMD) and luminosity functions (LF) with large statistics and small photometric errors from the Asymptotic Giant Branch (AGB) and Red Giant Branch (RGB) tip down to $\sim 0.15M_{\odot}$. This is the most extended and complete LF so far obtained for the galactic bulge. Similar near-IR data for a disk control field were used to decontaminate the bulge CMDs from foreground disk stars, and hence to set stronger constraint on the bulge age, which we found to be as large as that of Galactic globular clusters, or $\gtrsim 10$ Gyr. No trace is found for any younger stellar population. Synthetic CMDs have been constructed to simulate the effect of photometric errors, blending, differential reddening, metallicity dispersion and depth effect in the comparison with the observational data. By combining the near-IR data with optical ones, from the Wide Field Imager at the ESO/MPG 2.2m telescope, a disk-decontaminated ($M_K, V-K$) CMD has been constructed and used to derive the bulge metallicity distribution, by comparison with empirical RGB templates. The bulge metallicity is found to peak at near solar value, with a sharp cutoff just above solar, and a tail towards lower metallicity that does not appreciably extend below $[M/H] \sim -1.5$.

Key words. The Galaxy: bulge; Stars: C-M diagrams, luminosity function

1. Introduction

Galactic spheroids, i.e., elliptical galaxies and the bulges of spiral galaxies, contain a large fraction, probably the majority, of all the stellar mass in the local universe (Persic & Salucci 1992; Fukugita, Hogan, & Peebles 1998). Understanding their formation and evolution is therefore

crucial to understand galaxy formation in general, and to reconstruct the whole cosmic star formation history. However, it is only in the bulge of our own Galaxy that we can resolve the stellar population all the way to the bottom of the main sequence (MS), construct accurate color-magnitude diagrams (CMD) and luminosity functions (LF), and then address a series of issues of great importance for a better understanding of galactic spheroids in general. Such issues include the direct measure of some of the fundamental ingredients of galaxy models, like the initial mass function (IMF), the mass-to-light ratio and

[★] Based on observations collected at the European Southern Observatory, La Silla, Chile, obtained from the ESO/ST-ECF Science Archive Facility, and on observations with the NASA/ESA Hubble Space Telescope, obtained at the Space Telescope Science Institute, operated by AURA Inc. under contract to NASA

quantities such as the stellar age and metallicity distributions (MD).

Efforts in these directions have been quite numerous in recent years, and reviewing all of them is well beyond the scope of this paper. However, here are briefly mentioned some of the most recent attempts at determining the age, IMF and MD of the bulge stellar population.

The only published study of the bulge MD based on high resolution ($R=17,000$) spectra remains that by McWilliam & Rich (1994; hereafter M&R). They analyzed a sample of 11 red giants in Baade's Window, and used these data to re-calibrate a previous bulge MD based on low resolution spectra for 88 stars (Rich 1988). The resulting MD is centered around $[\text{Fe}/\text{H}]=-0.2$, with some 34% of the stars above solar metallicity, and no stars below $[\text{Fe}/\text{H}]\simeq -1.3$.

The bulge MD has also been derived using lower resolution spectra. Sadler et al. (1996) measured line strength $\langle \text{Fe} \rangle$ indices in low resolution ($R \sim 1000$) spectra of a sample of 322 bulge giants. These indices were calibrated vs. $[\text{Fe}/\text{H}]$ following Faber et al. (1985). Although the derived $[\text{Fe}/\text{H}]$ abundances for the few stars in common with M&R are in good agreement, the global MD by Sadler et al. (1996) is symmetric around $[\text{Fe}/\text{H}]=0$, and shows a population of stars with metallicity above solar more prominent than in any other study, which may result from having applied the $\langle \text{Fe} \rangle$ vs. $[\text{Fe}/\text{H}]$ calibration beyond its range of validity. More recently, Ramirez et al. (2000) derived the bulge MD by measuring the equivalent width of Ca, Na and CO lines in a sample of 110 M giants observed with resolutions from $R \sim 1300$ to 4800. They converted equivalent widths into $[\text{Fe}/\text{H}]$ by means of the Frogel et al. (2001) calibration, based on Galactic globular clusters (GCs) of independently known $[\text{Fe}/\text{H}]$. This assumes that the α -element enhancement of the bulge is the same as that of the clusters. The MD obtained in this case is similar to that of M&R, but with a sharper peak at $[\text{Fe}/\text{H}]=0$. The appreciable differences among the MDs derived in these studies are likely to arise from uncertainties in the calibration of the low resolution indices, that may introduce important systematics.

Dating bulge stars is complicated by several factors, such as crowding, depth effects, variable reddening, metallicity dispersion, and contamination by foreground disk stars. From WFPC1 observations of the bulge field known as Baade's Window, Holzman et al. (1993) inferred a dominant intermediate age component in the Galactic bulge. Shortly after the refurbishment of HST, two metal rich globular clusters of the bulge (NGC 6528 and NGC 6553) were observed with WFPC2 (Ortolani et al. 1995, hereafter Paper I). These clusters are respectively at $\sim 4^\circ$ and $\sim 6^\circ$ from the galactic center, and their overall metallicity $[\text{M}/\text{H}]$ is about solar (Barbuy et al. 1999; Cohen et al. 1999), close to the average for stars in Baade's Window (M&R). Like most other clusters within ~ 3 kpc from the Galactic center, they belong to the population of bulge globular clusters that have age, kinematical properties and metallicity distribution that are indistinguishable

from those of bulge stars (e.g., Minniti 1995; Paper I; Coté 1999). Hence, we do not hesitate to refer to them as *bulge globular clusters* (see also Forbes, Brodie & Larsen 2001; Harris 1976, 2001; Zinn 1996). In the case of NGC 6528 and NGC 6553 the bulge membership is also confirmed by the proper motion of the two clusters, in both cases well within the proper motion distribution of bulge stars (Zoccali et al. 2001a; Feltzing, Johnson, & de Cordova 2002). In Paper I it was shown that *i*) the two clusters have virtually identical CMDs, indicating that they have the same age and metallicity; *ii*) their magnitude difference between the horizontal branch (HB) *clump* and the MS turnoff is virtually identical to that of the inner halo globular cluster NGC 104 ($[\text{Fe}/\text{H}]=-0.7$), and *iii*) the LF of NGC 6528 (the least reddened of the two clusters) is virtually identical to the LF of bulge stars in Baade's Window, when allowance is made for the distribution of bulge star distance along the line of sight. From all these evidences Ortolani et al. concluded that *i*) the bulge underwent rapid chemical enrichment to solar abundance and beyond, very early in the evolution of the Milky Way (MW) Galaxy; *ii*) the bulk of bulge stars formed nearly at the same time as the halo globular clusters, and *iii*) no more than $\sim 10\%$ by number of the bulge population can be represented by intermediate age stars. These conclusions have been further strengthened after a statistical decontamination of the bulge CMD from the foreground disk stars (Feltzing & Gilmore 2000).

Dating the bulge via the MS turnoff also allows to check the usefulness of asymptotic giant branch (AGB) stars brighter than the red giant branch (RGB) tip as age indicators. Indeed, being such AGB stars much brighter than the MS turnoff, they have often been used in the attempt to date other galactic spheroids (such as M32 and the bulge of M31), sometimes inferring intermediate ages for some of these systems (e.g. Davidge and Nieto, 1992; Freedman 1992; Elston and Silva, 1992). However, the existence of AGB stars brighter than the RGB tip does not ensure a population to be of intermediate age: the old, metal rich ($[\text{Fe}/\text{H}] \gtrsim -0.7$) globular clusters of the MW bulge and inner halo (such as, e.g., NGC 6553 and NGC 104) do indeed contain some AGB stars that are ~ 1 magnitude brighter than the RGB tip (Frogel and Elias 1988; Guarnieri, Renzini, & Ortolani 1997). In any event, the RGB+AGB luminosity function conveys important information concerning the stellar population of the bulge, and its better understanding is important for the interpretation of the observations of nearby spheroids.

At the opposite extreme of the luminosity range, the LF of the lower MS is the only part of the LF that depends on the IMF, and therefore it allows the determination of this important property of stellar populations. Recent near-infrared data obtained with HST+NICMOS, have provided the deepest ever J, H photometry in the bulge, and allowed the determination of the IMF from $\sim 1M_\odot$ down to $\sim 0.15M_\odot$ (Zoccali et al. 2000, hereafter Paper II). The IMF resulted to be quite *flat*, with a slope -1.33 ± 0.07 (compared to -2.35 for the Salpeter IMF),

with a hint of a steepening toward the high mass end (see also Holzman et al. 1998).

The study of the NICMOS field extended to only 408 square arcsec¹, and therefore the number of stars on the upper MS is too small to allow any reliable location of the MS turnoff, while the evolutionary stages beyond the turnoff are not sampled at all. Thus, in Paper II an attempt was made to extend the main sequence LF to the evolved stars, using near-infrared data from the literature. A *complete* LF, extending from the bottom of the MS all the way to the AGB, was constructed by matching the NICMOS luminosity function of the lower MS, to the Tiede, Frogel & Terndrup (1995) LF extending from slightly above the turnoff to slightly above the HB, and finally to the Frogel & Whitford (1987) LF for the bulge M giants above the HB. While the resulting composite LF was constructed with the best data available in each luminosity range, several limitations were also obvious. Specifically, the MS turnoff region was not well sampled by neither the NICMOS data from Paper II (too few stars in the small field), nor by the Tiede et al. LF (not deep enough to reach the turnoff). Moreover, the upper RGB and AGB from Frogel & Whitford (1987) included only the M stars selected from an objective prism survey, hence omitting any luminous K giants that may be present in the explored bulge field. Finally, the NICMOS observations were conducted in a field 6° from the Galactic center, while the two other datasets were relative to Baade’s Window, at 4° from the center.

In this paper we present a thorough attempt at overcoming the current limitations of the available CMDs and LFs of the bulge, thereby producing *state of the art* CMDs and LFs used for new determinations of the age and metallicity distribution of the bulge. This approach is based on new near-IR (J, H, K_s) data obtained with SOFI at the ESO New Technology Telescope (NTT), as well as on optical (V, I) data obtained with the Wide Field Imager (WFI) at the ESO/MPG 2.2m telescope. These data are then coupled with the NICMOS data from Paper II for the lower MS, and with the 2MASS near-IR data for the upper RGB and AGB (van Dyk, 2000; Carpenter, 2001; and references therein).

The paper is organized as follows: Observations and data reduction procedures are presented in Section 2, the CMDs are displayed and discussed in Section 3, while Section 4 is devoted to the derivation of the metallicity distribution. The luminosity function of the bulge is constructed and discussed in Section 5, while Section 6 is devoted to determining the age of the bulge, and Section 7 to a discussion of the RGB tip in the different bands. Finally, the main results are again summarized in Section 8, along with some inferences on the formation of the Galactic bulge and spheroid, also in the context of the current evidence on the formation of galactic spheroids in general.

2. Observations and Data Reduction

The data presented here come from the combination of near-IR J, H, K_s observations conducted with SOFI@NTT, implemented with public data from the 2MASS survey and with NICMOS data from Paper II, plus optical V, I images taken with the WFI@2.2m as part of the EIS PRE-FLAMES survey (Momany et al. 2001; and references therein), and retrieved from the ESO archive. The relevant technical information about the observations are reported in Table 1, while details on the observational strategy and data reductions are described here below.

2.1. Near-IR data

A bulge mosaic field centered at $(l, b) = (0.277, -6.167)$ (RA=18:11:13, DEC=-31:43:49; J2000) was observed with SOFI@NTT, through the filters J, H, K_s , in the nights of 9–12 June 2001. This particular field was selected for the present study because it includes the field already covered by the NICMOS observations (Paper II), which in turn was chosen for having a reddening ($E(B-V) = 0.47$) as low as that of the most widely studied Baade’s Window while being less crowded. Indeed, being $\sim 2^\circ$ further away from the Galactic center the density of stars is lower by a factor ~ 2 , which allows more accurate photometry especially at very faint magnitudes.

In order to optimize the photometry of both the turnoff region and the upper RGB, the observations were split in short and long exposures, each with a different field objective, and therefore mapping areas of different sizes. For a good sampling of RGB+AGB stars, short exposures were obtained for a $8'3 \times 8'3$ region, with a mosaic of four fields of the low resolution camera, which has a pixel size of $0'292$ and field of view of $4'9 \times 4'9$ (hereafter SOFI-LARGE field). In order to better sample the PSF, a second mosaic of four deeper exposures mapping a smaller area ($3'9 \times 3'9$) was secured with the same camera coupled with the focal elongator, therefore yielding a pixel size of $0'144$ and a $2'5 \times 2'5$ field of view (hereafter SOFI-SMALL field). An overlap of $\sim 20\%$ was always present among the four fields of each mosaic.

Exposures of a disk control field located at $(l, b) = (30, 0)$ (RA=19:07:32, DEC=-05:19:57) were also obtained for one pointing of the large field camera in order to estimate the disk contribution to the bulge CMD (Section 4).

Each of the deep exposures, both for the disk and the bulge field, was obtained with detector setup DIT=6 NDIT=5 (i.e., every frame was the average of 5 exposures of 6 sec. each), while for the shallow ones we used DIT=1.2 and NDIT=5². Both of them were repeated with a random dithering pattern until reaching the exposure time listed in Table 1. Both sky transparency and seeing were somewhat variable during the run, and for this reason the

¹ The size of the NICMOS field was erroneously quoted as 506 square arcsec in Paper II.

² See the SOFI User Manual for a more detailed explanation of the instrument setups:
<http://www.eso.org/lasilla/Telescopes/NEWNTT/scfi>

Table 1. Log of the observations

Date	Object	Camera	RA	DEC	Filter	Exptime
11 Jun 2001	bulge	SOFI-LARGE	18:11:05.0	-31:45:49	J	36s
"	"	"	"	"	H	36s
"	"	"	"	"	Ks	36s
"	"	"	18:11:22.0	-31:45:49	J	36s
"	"	"	"	"	H	36s
"	"	"	"	"	Ks	36s
"	"	"	18:11:22.0	-31:41:49	J	36s
"	"	"	"	"	H	36s
"	"	"	"	"	Ks	36s
"	"	"	18:11:05.0	-31:41:49	J	36s
"	"	"	"	"	H	36s
"	"	"	"	"	Ks	36s
11-12 Jun 2001	bulge	SOFI-SMALL	18:11:05.0	-31:45:49	J	1180s
"	"	"	"	"	H	1530s
"	"	"	"	"	Ks	2880s
9-11 Jun 2001	"	"	18:11:13.5	-31:45:49	J	1200s
"	"	"	"	"	H	1020s
"	"	"	"	"	Ks	1920s
9-11 Jun 2001	"	"	18:11:13.5	-31:43:49	J	1200s
"	"	"	"	"	H	1020s
"	"	"	"	"	Ks	1920s
9-11 Jun 2001	"	"	18:11:05.0	-31:43:49	J	1200s
"	"	"	"	"	H	1020s
"	"	"	"	"	Ks	1920s
11 Jun 2001	disk	SOFI-LARGE	19:07:32.0	-05:19:57	J	600s
"	"	"	"	"	H	510s
"	"	"	"	"	Ks	960s
15 Apr 1999	bulge	WFI	18:10:17.0	-31:45:16	V	20s
"	"	WFI	"	"	V	2×300s
"	"	WFI	"	"	I	20s
"	"	WFI	"	"	I	3×300s

total exposure times on different fields were adjusted in order to compensate for these effects. The typical seeing during the observations was $0''.80 \pm 0''.15$.

Images were pre-reduced using standard IRAF routines. A sky image, obtained by median combination of the dithered frames of each filter, was subtracted from each frame. Flat fielding was then performed using the "SpecialDomeFlat" template which applies the appropriate illumination corrections, as described in the SOFI User Manual. Finally, all the dithered frames obtained in a sequence were averaged in a single image for each filter. In what follows we will call "frame" the combination of each of these sets.

Standard photometry, including PSF modeling, was carried out on each frame using the DAOPHOTII photometry package (Stetson 1987). We used all the stars identified in each frame to obtain the coordinate transformations among the frames. These transformations were used to register the frames and obtain a median image. The latter, having the highest S/N, was used to create the star list, by means of a complete run of DAOPHOTII and ALLSTAR. The final star list, together with the coordinate transformations, was finally used as input for ALLFRAME (Stetson 1994), for the simultaneous PSF-fitting photometry of all the frames of each field.

Only one of the four half-nights assigned to this programme was photometric. During that night we observed several standards from the Persson et al. (1998) catalog,

three of which just before and after one of the bulge fields observed with SOFI-SMALL. This field was calibrated by means of the standard stars, whose frames were pre-processed in the same way as the science ones. Aperture photometry within a radius of 5.8 arcsec was obtained for the standard stars, and aperture corrections determined using some bulge isolated and unsaturated stars were applied to the PSF instrumental magnitudes of the bulge field. The calibration equations obtained from the standard stars were then applied to the magnitude of the bulge stars, neglecting the color term due to the very small color range of the near-IR standard stars. Having calibrated one bulge field, all the others were registered to the same photometric system by comparison of the common stars: a single large field included the whole mosaic of four small fields, and there was always $\sim 20\%$ overlap among the four fields of each mosaic.

The whole bulge area mapped with SOFI is also included in the 2MASS near-IR survey (Carpenter 2001), whose second incremental release is publicly available on the WEB³. Figure 1 shows the comparison between the J, H, K_s magnitudes from our calibrated photometry and the same quantities for the stars in common with the 2MASS point source catalog. The latter has a limit magnitude of $K_s \sim 15$, therefore only the stars measured in one of the four SOFI-LARGE fields (i.e., in the short ex-

³ <http://irsa.ipac.caltech.edu/applications/2MASS>

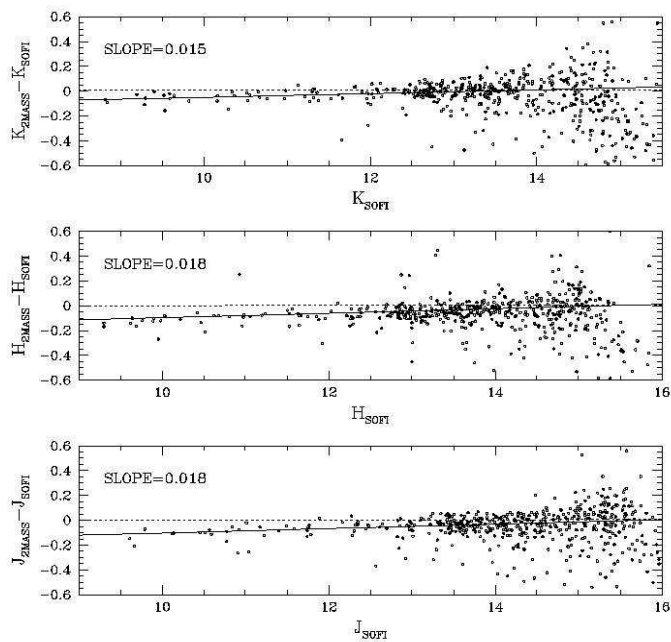


Fig. 1. Comparison between the SOFI photometry and that from the 2MASS survey, for the stars in common. The solid line is the least square fit to the data, while the dotted one is the relation found by Carpenter (2001).

posures) are plotted in this figure. The solid line represents a least square fit to the data, while the dotted one is the relation between the 2MASS and the Persson et al. (1998) photometric system (Carpenter 2001). The latter is based on 2MASS observations of 82 standard stars from Persson’s catalog.

A trend with magnitude is clearly visible in Fig. 1, with the difference between the two photometries being zero at the faintest limit but increasing up to ~ 0.1 mag at the brightest end in J and H , while remaining quite small ($\lesssim 0.05$ mag) in K_s . Such a behavior points to a non-linearity effect in one of the two detectors. To our knowledge neither the 2MASS nor the SOFI measurements should be affected by non-linearity; in particular the SOFI detector has been tested to be linear within 2% up to 10,000 ADU (cf. the SOFI User Manual), and only the three brightest stars in this plot have counts above this limit. We are then left with no explanation for the trend seen in Fig. 1, but none of our conclusions relies on an accuracy better than ~ 0.1 in the magnitudes. Moreover, if the error is in our measurements and not in the 2MASS ones, the trend is identical in the J and H bands, therefore it would affect the magnitudes but not the $J - H$ color we used to construct the CMD shown in Section 3.

The disk control field was not observed during the photometric night, therefore the only way we had to calibrate its CMD was to rely on the comparison with 2MASS. However, given that our main interest was to put the disk stars in the same photometric system as the bulge ones, we determined the calibration transformations be-

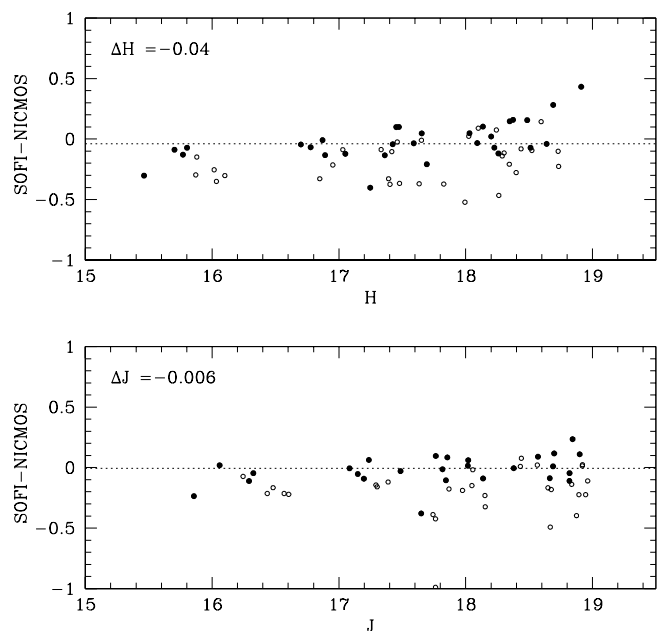


Fig. 2. Comparison between the SOFI photometry presented here and the deep NICMOS photometry from Paper II, for the stars in common. Open circles refer to stars that may be affected by blending in SOFI frames.

tween our disk instrumental magnitudes and 2MASS, but then also applied the small differences shown in Fig. 1, in order to try and keep consistency between the disk and bulge calibrated photometry.

One of the goals of this project is to obtain a complete luminosity function for the galactic bulge, from the RGB tip down to the faintest stars ($0.15M_{\odot}$) measured with NICMOS. Therefore, it is crucial to make sure that the NICMOS photometry is consistent with that obtained here with SOFI, especially given the large uncertainties in the NICMOS calibration (Stephens et al. 2000). Figure 2 shows the differences in J and H for the stars in common between the two data sets. Given the large difference in spatial resolution between SOFI and NICMOS, this comparison may be affected by systematics due to the presence of close pairs of stars resolved by NICMOS but not by SOFI. For this reason, different symbols (filled) were adopted in Figure 2 for the stars whose positions matched within 0.5 SOFI pixels. These stars are less likely to be blends, because the presence of a companion *resolved by NICMOS* would likely result in a displacement of the star centroid. The median differences, in J and H , between the common stars, if only the *bona fide* single stars are considered, are $\Delta J = -0.006$ and $\Delta H = -0.04$ as shown in the figure labels. If all the common stars were considered, the median differences would be anyway negligible for our purposes: $\Delta J = \Delta H = -0.09$.

Completeness estimates were determined via artificial-star experiments. A total of about 3500 stars were added to the original SOFI frames, both for the bulge and for the

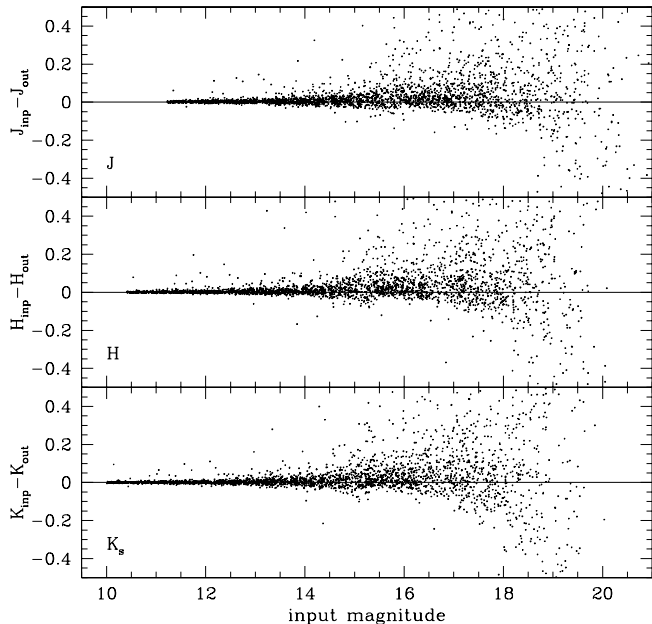


Fig. 3. Difference between the input and the output magnitude of the artificial star experiments on the SOFI frames. The results obtained for the SOFI-LARGE and SOFI-SMALL frames were matched at $J = 16$ as in the photometry of the real stars.

disk fields, with magnitudes and colors consistent with the RGB+MS instrumental fiducial lines. In order to avoid to artificially increase the crowding, at the same time optimizing the CPU time, in each independent experiment the artificial stars were added along the corners of an hexagonal grid, as explained in Paper II. As usual, photometry of the artificial frames was performed following the same procedures as for the original ones.

Figure 3 shows the results of these experiments, as the difference between the input and output magnitude of the artificial stars in each filter.

Note that the distribution is asymmetric about the zero, as occasional blendings result in brighter output magnitudes compared to the input ones. However, the ridge line (i.e., the peak of the distribution) remains close to zero up to $J \sim 18$, and therefore the estimate of the turnoff magnitude, from the CMD ridge line is not affected by blending. We expect instead the luminosity function to be affected (see Section 5.1). The simulations have shown that the SOFI photometry is more than 50% complete above $J \sim 19$ and $H = K_s \sim 18$.

2.2. Optical data

A 34×33 arcmin bulge field including the whole area mapped with SOFI was observed with the wide field imager WFI@2.2m telescope, as part of the EIS PRE-FLAMES programme (Momany et al. 2001). The V and I raw frames have been retrieved from the public ESO

archive, while the pre-processed images were not released yet. The frames were taken under very good seeing conditions, with a PSF FWHM of $0''.6$, as measured on the frames. Details about the observations are given in Table 1. Science images were de-biased and flatfielded by means of standard IRAF routines, using a set of sky flat-fields taken the same night.

The photometry for each of the 8 WFI chips was performed separately, in order to properly model the PSF variation across them. As usual, complete photometry and PSF modeling were carried out on each of the I and V frames, and then coordinate transformations were calculated among them in order to obtain a median frame to use for a more complete star finding. The star list obtained in this way was then used as input for ALLFRAME, which performed simultaneous PSF fitting photometry on the 3 V and 4 I frames. The whole procedure was repeated for each of the 8 chips.

Calibration to the Johnson photometric system was performed by means of a set of Landolt (1992) standard fields observed the same night through the 8 WFI chips. The number of standard stars present in each of these fields has been recently increased by Stetson (2000), allowing us to measure ~ 40 standard stars per chip. A zero point and a color term were determined separately for each chip. The color terms were then averaged, and new zero points were calculated imposing the former to be fixed. Variations $\lesssim 0.1$ mag have been found among the photometric zero points of different chips.

Completeness estimates were determined for the WFI data in the same way described above for the SOFI ones. WFI data are more than 50% complete above $I \sim 22.5$, and $V \sim 23$.

3. The Color Magnitude Diagram

3.1. Near-IR CMD

Figure 4 shows the near-IR CMD of all the stars measured in the bulge field. The jump in the number of stars at $J = 16$ is due to stars brighter than $J = 16$ having been sampled from the 8.3×8.3 SOFI-LARGE field, while fainter stars have been measured with the larger angular resolution and deeper exposures of the SOFI-SMALL field, which mapped a 3.9×3.9 area.

The bulge HB red clump is visible at $J \sim 14$ and $J - H = 0.6$, partially merged into the RGB. The large magnitude spread of the HB is due to a combination of differential reddening, metallicity dispersion and depth effect. These factors also cause the HB clump to merge vertically with the RGB *bump*, expected to be located ~ 0.7 magnitudes fainter in J . The RGB bump (Iben 1968; Rood 1972; Salaris, Cassisi & Weiss 2002) is predicted to be very populated in a high metallicity system as the bulge, and would have itself a large magnitude spread due to the same depth and reddening effects mentioned for the HB clump.

The bulge turnoff is clearly visible at $J \sim 17.5$ and $J - H \sim 0.4$, while the almost vertical sequence depart-

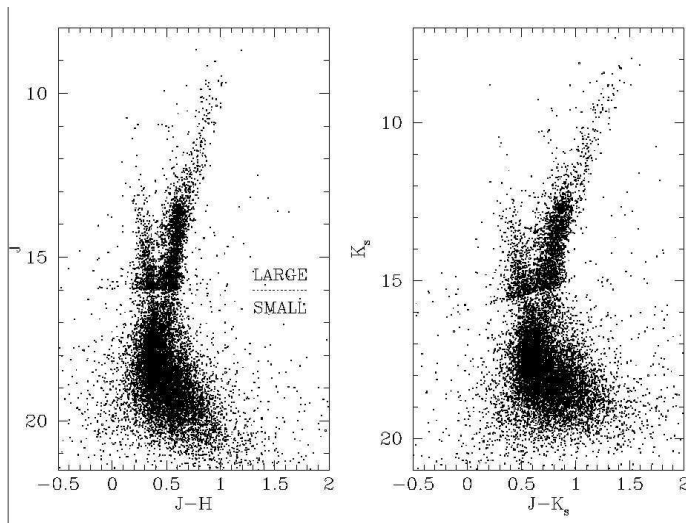


Fig. 4. J, H (left) and J, K_s (right) CMD of the bulge stars imaged with SOFI. In both panels, stars brighter than $J = 16$ come from the $8'.3 \times 8'.3$ area mapped with short exposures and the SOFI-LARGE field, while fainter stars were measured in a 3.9×3.9 arcmin area observed with the SOFI-SMALL field.

ing from near the bulge turnoff and extending upwards and bluewards is due to foreground main sequence stars belonging to the disk, widely dispersed along the line of sight (Ng & Bertelli 1996).

Fig. 5a shows the CMD of the bulge field with superimposed a 1 Gyr isochrone, for a solar metallicity population, adopting a distance modulus of $(m - M)_0 = 14.47$ and a reddening of $E(B - V) = 0.45$ (see below). Clearly, a population of young stars physically located inside the bulge, would be definitely bluer than the vertical sequence of disk stars. The disk field, 30° away from the Galactic center, was used to statistically decontaminate from the foreground disk stars the bulge CMD shown in Fig. 5a. Small differences in the disk stellar population may be expected between the two lines of sight. Yet, the results have shown that the procedure is indeed quite effective. The CMD of the disk control field for an area of 24 square arcmin is shown in Fig. 5b. The difference in reddening between the two fields was compensated by shifting the disk CMD shown in Fig. 5b by 0.17 mag in $J - H$ so as to match the color location of the blue disk sequences, and in magnitude by the corresponding $A_J = 3.06E(J - H)$ extinction (Cardelli, Clayton & Mathis 1989). A region of the CMD free of bulge stars was then selected in order to normalize the number of disk stars observed in the disk field to the number of disk stars contaminating the bulge field. This region is indicated by the box in the upper left region of the CMD in Fig 5a. This normalization is correct only if no bulge star is present in the box.

There are 91 stars in the box of the disk control field, which is 4.5 times less than in the corresponding box of the bulge SOFI-LARGE field. Therefore, 4.5 stars have been subtracted from the brighter region ($J < 16$) of the

bulge CMD for each star seen in the disk CMD. Since the fainter part of the CMD ($J > 16$) was derived from the SOFI-SMALL field, the 4.5 scaling factor was divided by the ratio of the SOFI-LARGE to SMALL field area (4.6). Hence 0.98 stars have been subtracted from the fainter part of the CMD for each star in the disk control field.

For each disk star in the disk CMD (Fig. 5b) we picked up the *closest* star in the bulge CMD (see below), and subtracted it according to the normalization factors given above, and to the slightly different completeness of the two fields. The *distance* on the CMD from a disk star to each bulge star was defined as:

$$d = \sqrt{[7 \times \Delta(J - H)]^2 + \Delta J^2}.$$

The color difference has been enhanced by a factor of 7 because the color is much less sensitive than the magnitude to physical differences (in the distance, reddening or mass) between a given disk star in the control field, and another disk star along the bulge line of sight. The resulting, clean CMD of the bulge is shown in Fig. 5c, while the CMD of the stars statistically removed from the bulge CMD is shown in Fig. 5d. Also shown in this panel are the fiducial ridge line, helping the eye to identify the mean branches of the bulge CMD, and the brighter and fainter limits of our turnoff magnitude estimate ($J = 17.65 \pm 0.2$).

The clumpy appearance of the RGB of Fig. 5d is due to the poor statistics in this region of the disk CMD since for each disk star we had to subtract 4.5 times more stars in the bulge field. Hence for each disk star a small “cluster” of close stars was subtracted from the bulge CMD. In the attempt to minimize this effect we actually subtracted every *other three* closest stars in the region $J < 16$. We expect a negligible effect on the 0.25 magnitude bins of the luminosity function discussed in the next Section.

The 2MASS catalog was used to improve the statistics for the bright part of the CMD and of the luminosity function. Note however, that the $\sim 4''$ resolution of 2MASS is significantly worse than either the SOFI or WFI data. This complicates somewhat the cross identifications with the SOFI and WFI databases, and crowding effects are much more severe since two objects closer than $\sim 4''$ are counted as one in the catalog.

From the 2MASS point source catalog we extracted near-IR data for two large areas, 31×31 arcmin each, containing our bulge and disk field, respectively. A procedure identical to that described above for the SOFI data has been applied to the bulge CMD of Fig. 6a in order to statistically decontaminate bulge from disk stars, using the disk CMD shown in Fig. 6b. Note that since the disk and bulge field areas are now identical, the scaling factor for the decontamination (determined within a box similar to that shown in Fig. 5) is now very close to 1.

The result is again very satisfactory (Fig. 6c,d) for stars brighter than $J \sim 13$. For fainter stars the decontamination is less effective because the magnitude and color spread of the disk and bulge CMD in Fig. 6 are quite different, due to the different drivers of the magnitude limits. Indeed, due to the low spatial resolution of the 2MASS

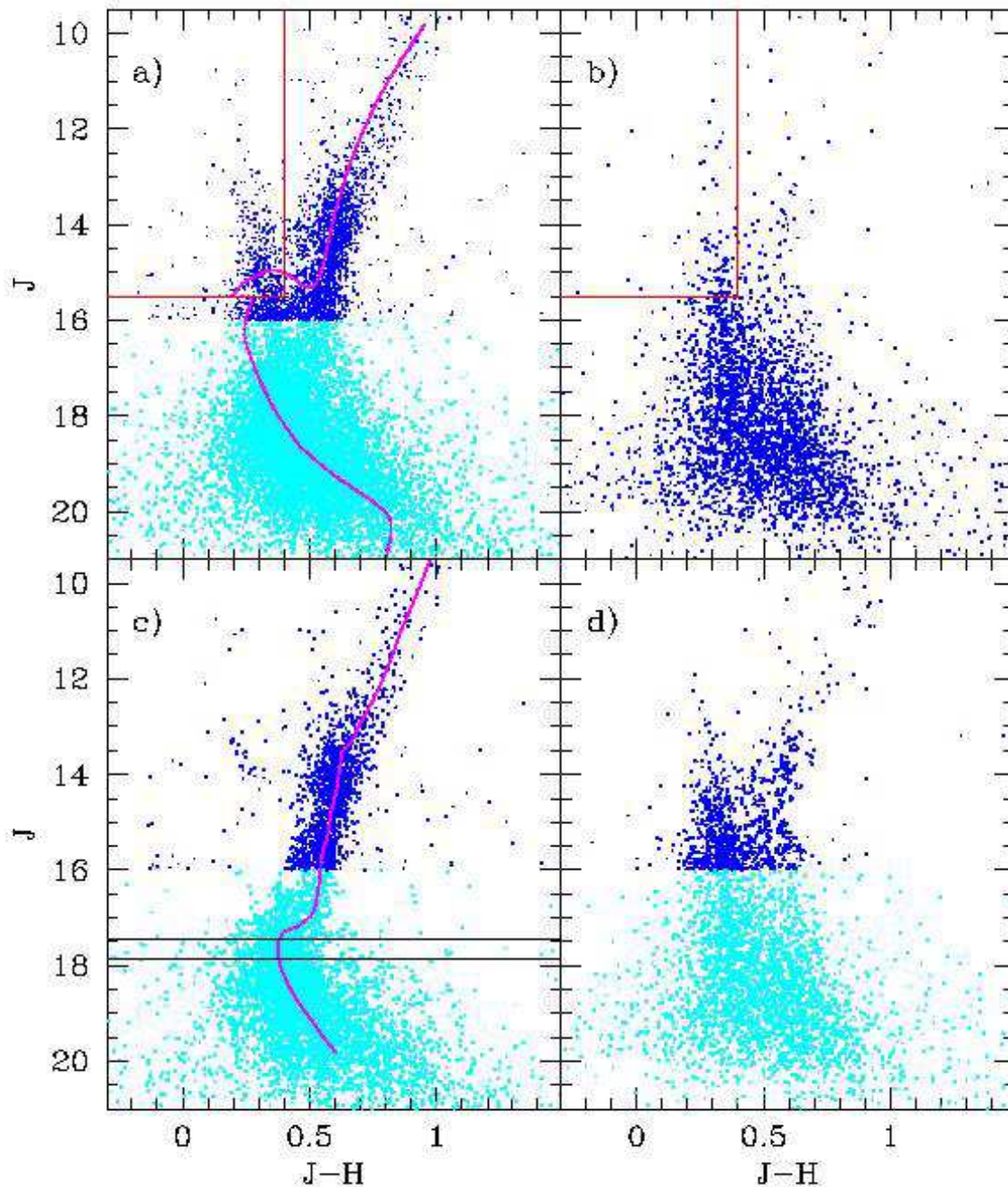


Fig. 5. *a)* The CMD of the bulge field. The solid line is the 1 Gyr isochrone for a solar metallicity population. *b)* CMD of the disk control field in the direction $(l, b) = (30, 0)$. The region inside the box has been used to normalize the number of disk stars seen through the bulge line of sight. *c)* CMD of the bulge field as statistically decontaminated from the disk population. The horizontal lines locate the main sequence turnoff at $J = 17.65 \pm 0.2$. The ridge line of the CMD is also shown. *d)* Stars that were subtracted from the bulge CMD in order to obtain the decontaminated CMD.

data, the photometry is limited by the crowding in the bulge field, and by the background noise (including sky) in the disk. However, in the following only the brightest stars ($J \lesssim 12$) of the 2MASS decontaminated bulge CMD will be used.

3.2. The Optical CMD

Figure 7 shows the $(I, V - I)$ CMD of the 883,417 stars measured in the 34×33 arcmin field of WFI@2.2m. The eight panels in this figure correspond to the eight CCD chips of the WFI mosaic, maintaining their relative spatial

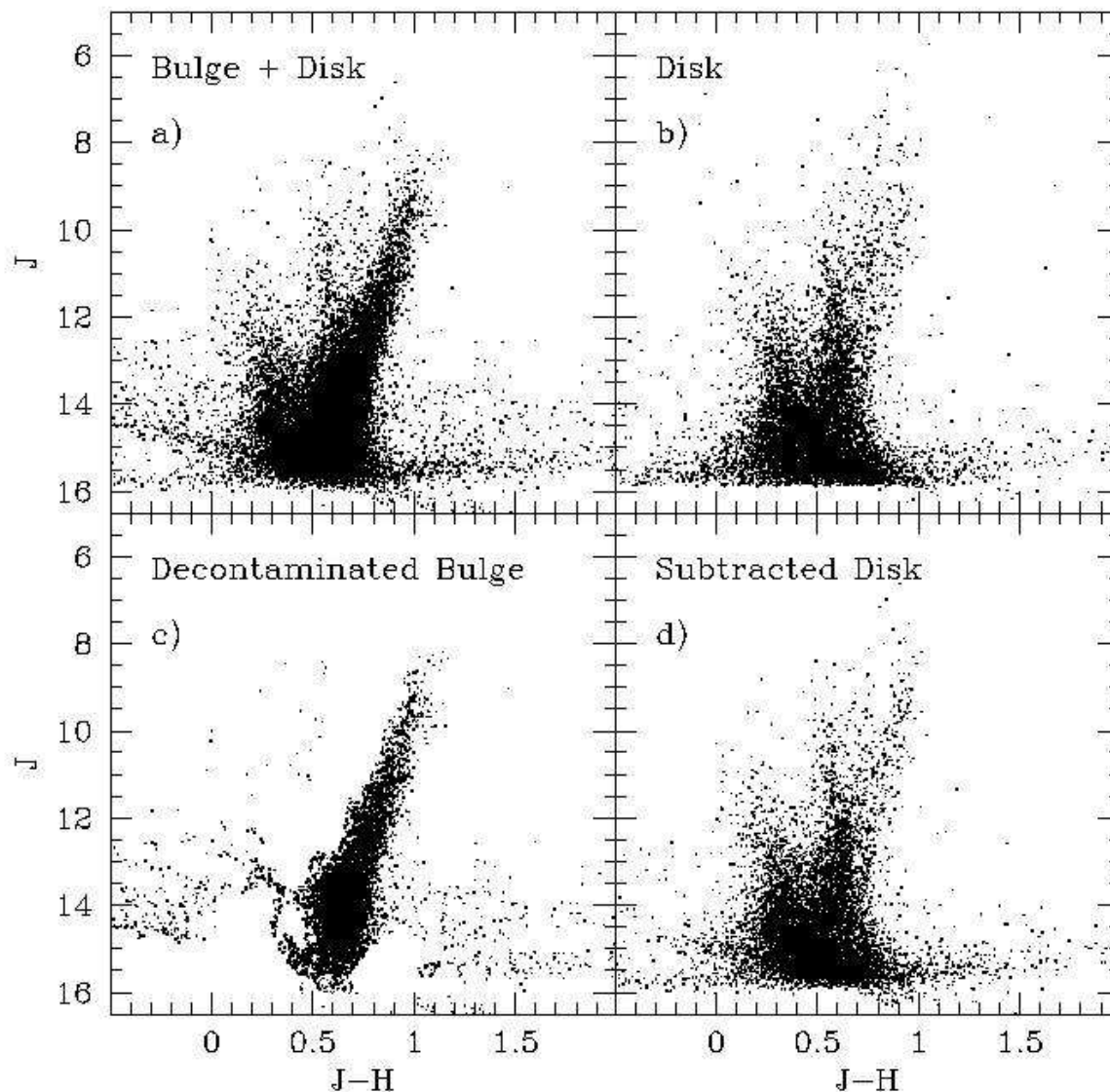


Fig. 6. CMDs of the bulge (panel *a*) and disk (*b*) fields as constructed from the 2MASS photometry. *c*) The bulge CMD after statistical decontamination from disk stars; *d*) *bona fide* disk stars subtracted from *a*) in order to obtain *c*).

position. The huge number of points per panel saturates the plot in the most populated areas, like the bulge main sequence ($I > 18$). The bulge turnoff is located around $I = 18$, while the main sequence of the foreground disk hits the bulge locus approximately midway between the turnoff and the base of the RGB. The HB red clump (merged with the RGB bump) is visible at $I \sim 14.5$ and $V - I \sim 1.8$, while the upper RGB (brighter than the HB) is extremely wide due to the bulge metallicity dispersion. Note, however, that the narrow sequence departing from the bulge HB and extending upward, almost vertically is due to the red clump of the disk stars, dispersed in magnitude as a result of their large spread in distance (and reddening). The bulge main sequence extends almost vertically in this plot, becoming very broad towards faint

magnitudes for the combination of photometric error and plot saturation, but its increasing skewness towards red colors is in fact due to the presence of the faint extension of the disk main sequence.

Although there is evidence for a bulge blue HB population in all the CMDs (with $V - I \simeq 0.5 \div 1$ and $I \simeq 15 \div 18$), note that chip#6 (panel f) contains the bulge globular cluster NGC 6558, already known to have a blue HB (Rich et al. 1998). The fact that the blue HB seen in this CMD belongs to the cluster becomes very clear when imposing a spatial selection around the cluster center. The other cluster features are not distinguishable from the bulge ones in this plot. A circular region of 2.4 arcmin radius, centered on NGC 6558, has been excluded from the following analysis. The radial trend of both cluster star counts and surface

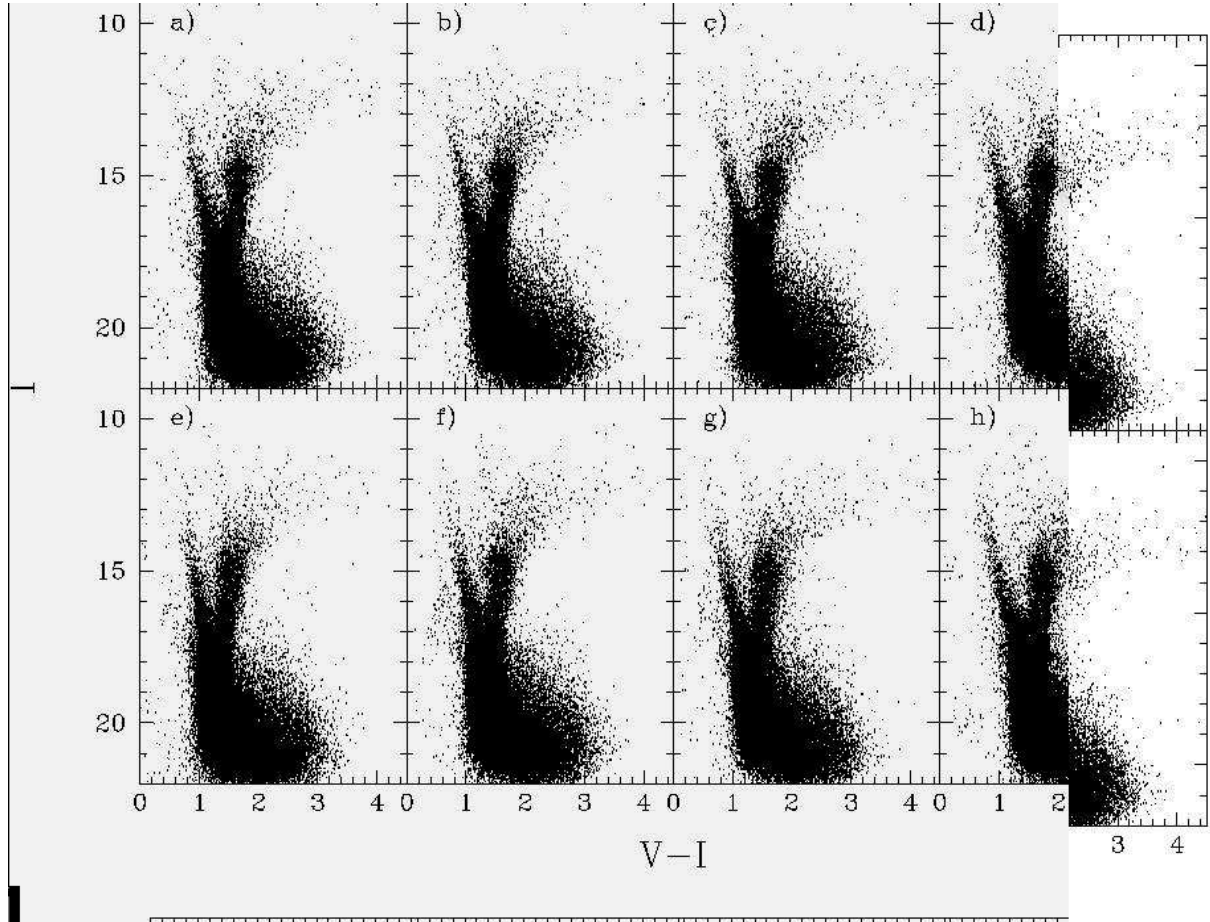


Fig. 7. The optical CMD of the bulge from the WFI data. Each panel corresponds to each of the $8K \times 8K$ CCD chips of the WFI camera.

brightness flattens to the background level well inside this radius, ensuring a negligible cluster contamination outside 2.4 arcmin.

For a better visibility of the bright portion of the CMD, Fig. 8 displays only stars brighter than $I = 16$, this time combining data from all the 8 chips of WFI. The disk main sequence is very prominent on the left side of the diagram, and is paralleled some ~ 0.8 mag redder in $V-I$ by the core helium burning *clump* sequence belonging to the same population. The bulge RGB and AGB occupy the right side of the diagram, and become very dispersed in their upper part due to the metallicity dispersion. The HB clump and the RGB bump are also indicated in the figure.

4. The Metallicity Distribution of the Bulge

From the combination of the optical (WFI) and near-IR (2MASS) decontaminated data, a $(M_K, V-K)$ CMD was obtained including $\sim 22,000$ stars with $M_K < 0.5$, and the result is shown in Fig. 9. A comparison with the fiducial line of the globular cluster NGC 6528 from Ferraro et al. (2000) immediately suggests that the mean metallicity of the bulge is virtually identical to that of this cluster, with a quite modest dispersion about this mean. This is demon-

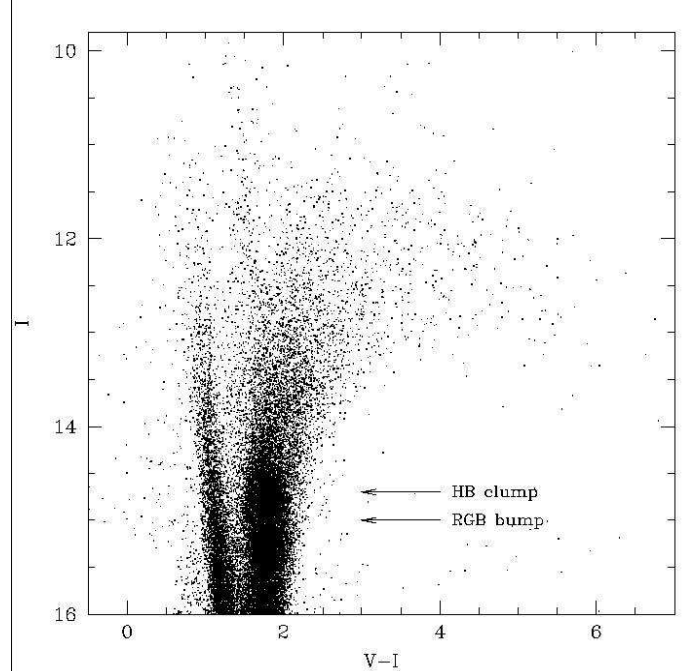


Fig. 8. The optical CMD for the bright stars combining the data in the whole WFI field. The location of the HB clump and the RGB bump is indicated.

Table 2. Globular Cluster used as RGB Templates

Cluster	[M/H]	$(m - M)_0$	$E(B - V)$
NGC 6528	-0.10	14.37	0.62
NGC 6553	-0.10	13.46	0.84
NGC 104	-0.57	13.32	0.05
NGC 6171	-0.88	13.95	0.31
NGC 6121	-1.06	11.68	0.35
NGC 6809	-1.59	13.82	0.10
NGC 7099	-1.84	14.71	0.01
NGC 4590	-1.90	15.14	0.04
NGC 7078	-1.92	15.15	0.09

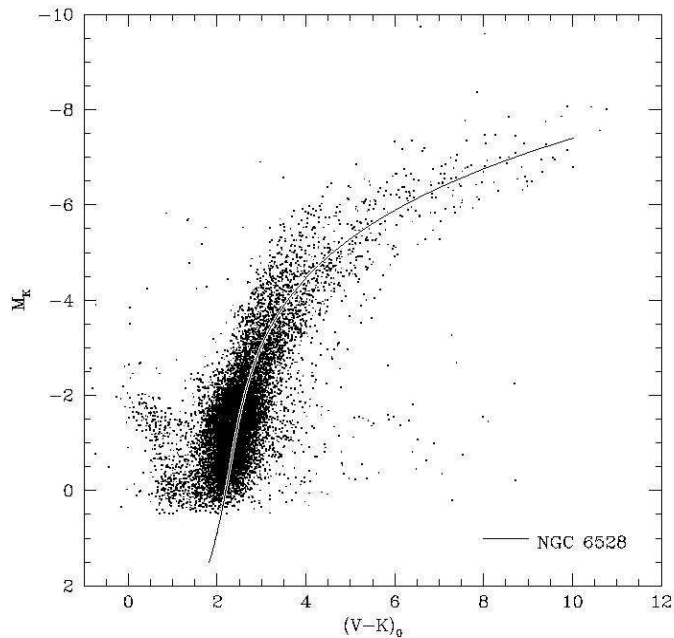


Fig. 9. Bulge CMD resulting from the combination of the optical WFI and near-IR 2MASS data. The line represents the fiducial locus of the globular cluster NGC 6528. The distance and reddening of the bulge field adopted for this comparison are $(m - M)_0 = 14.47$ and $E(B - V) = 0.45$, respectively, while for NGC 6528 it is assumed $(m - M)_0 = 14.37$ and $E(B - V) = 0.62$ (Ferraro et al. 2000).

strated by the slope of the giant branch of the cluster and of that of the bulge field being the same. (Note that the metallicity affects the *slope*, while the reddening causes a solid shift of the RGB.) Therefore, the metallicity of NGC 6528 (and that of the twin cluster NGC 6553) has a special importance in connection with our attempt at determining the bulge metallicity distribution. In Fig. 9, a distance modulus of $(m - M)_0 = 14.47 \pm 0.08$ (7.8 kpc) was adopted for the bulge, according to the most recent determination by McNamara et al. (2000) using RR-Lyrae and δ Scuti variables from the OGLE survey. The reddening of our bulge field relative to NGC 6528 can then be estimated from Fig. 9, and we obtain $E(B - V) = 0.45$, needed to

match the bulge and the cluster loci given the small difference in the two distance moduli. For NGC 6528 the corresponding quantities are given in Table 2. The large number of stars in the upper RGB of Fig. 9, coupled with the high sensitivity of the $(V - K)$ color to metallicity, and its very small sensitivity to a possible age dispersion, allows a determination of the bulge MD via the method described in Saviane et al. (2000).

4.1. The Method

The method is based on the construction of a family of hyperbolas in the plane $(M_K, V - K)$ suitable to represent a grid of upper RGBs from empirical template globular clusters, with known metallicities. Each hyperbola is represented by the expression:

$$M_K = a + b \times (V - K) + \frac{c}{(V - K) - d} \quad (1)$$

where the coefficients a, b, c and d are quadratic functions of the metallicity:

$$a = k_1[M/H]^2 + k_2[M/H] + k_3 \quad (2)$$

$$b = k_4[M/H]^2 + k_5[M/H] + k_6 \quad (3)$$

$$c = k_7[M/H]^2 + k_8[M/H] + k_9 \quad (4)$$

$$d = k_{10}. \quad (5)$$

Finally, the inversion of equation (1) gives a value of the metallicity for *each point* in the $(M_K, V - K)$ plane, hence for each bulge star.

Although in principle spectroscopic determinations may be more accurate, the photometric approach has the advantage of relying on high S/N quantities (i.e., the magnitudes of the brightest stars) and on large statistics. However, it is entirely differential, i.e., it depends on the accuracy of the metallicity assigned to the templates, which ultimately relies on spectroscopic determinations. The most complete and homogeneous grid of near-IR GC RGB templates presently available in the literature (Ferraro et al. 2000; see Table 2) includes 10 low reddening, nearby GCs with metallicity [M/H] between -1.92 and -0.1 . One cluster (NGC 6637) from the Ferraro et al. sample has been excluded from our calculations, for reasons explained below.

With the exception of the two most metal rich clusters (NGC 6528 and NGC 6553), for the GCs in Table 2 we adopted the iron abundance [Fe/H] from Harris (1996), and corrected it to [M/H] adopting an α -element enhancement $[\alpha/Fe]=0.3$ for clusters with $[Fe/H] < -1.0$, and $[\alpha/Fe]=0.20$ for more metal-rich clusters (Carney 1996; Salaris & Cassisi 1996). As emphasized earlier, the case of NGC 6528 and NGC 6553 is particularly important. A few stars in each of the two clusters have been observed at intermediate and high spectral resolution, but different groups have obtained quite discrepant results. For NGC 6528, Carretta et al. (2001)

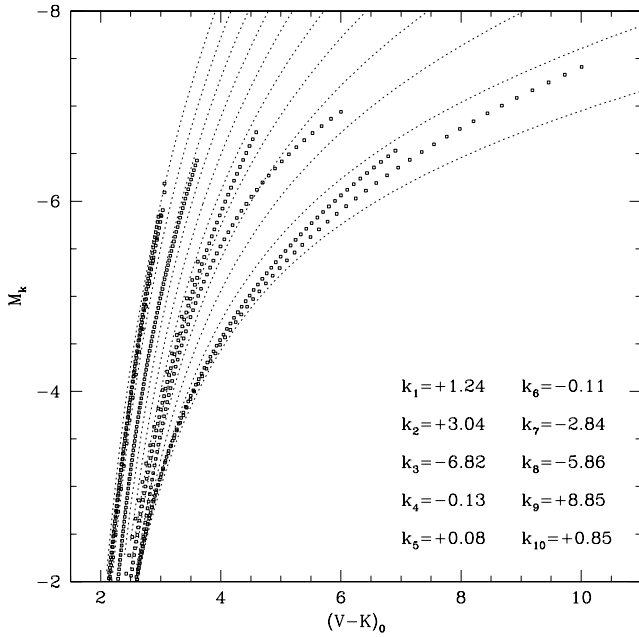


Fig. 10. The V, K RGBs of the template GCs published by Ferraro et al. (2000) (open squares), together with the analytical RGBs (dotted lines). The values of $[M/H]$ for the analytical RGBs go from solar to $[M/H] = -2.0$ in steps of 0.2.

and Coelho et al. (2001) report respectively $[Fe/H] = +0.07$ and -0.5 (the latter value coming from low-resolution spectra). For $[M/H]$ the same authors derive $+0.17$ and -0.25 , respectively. For NGC 6553 Barbuy et al. (1999) give $[Fe/H] = -0.55$ and $[M/H] = -0.08$, while Cohen et al. (1999) report $[Fe/H] = -0.16$, and Origlia, Rich & Castro (2002) give $[Fe/H] = -0.3$, with $[\alpha/Fe] = +0.3$. These discrepancies are uncomfortably large, and may hopefully disappear as soon as more high-resolution data are gathered at 8-10m class telescopes. For both clusters we finally adopt $[M/H] = -0.1$ (the value reported in Table 2) with the uncertainty of the resulting MD being dominated by the uncertainty of the metallicity of these two clusters.

Figure 10 shows the resulting grid of RGB loci: open squares represent the fiducial points extracted from the empirical templates, while the RGBs from the analytical interpolation are shown as dotted lines. The coefficients of the Equations 4–7 are listed inside the figure. The analytical RGBs are shown for metallicities ranging from $[M/H] = 0$ to $[M/H] = -2.0$, in steps of 0.2. All the empirical templates, with the exception of NGC 104 (third cluster from the right) follow very well the RGB shape trend of the analytical solution. We could find no obvious explanation for the apparent discrepancy of NGC 104: its CMD is quite populated in this region, and, being one of the best studied clusters, the adopted parameters (metallicity, reddening and distance) are rather robust. The near-IR observations of this cluster were done with the ESO/MPG 2.2m telescope mounting IRAC-2, an early IR array de-

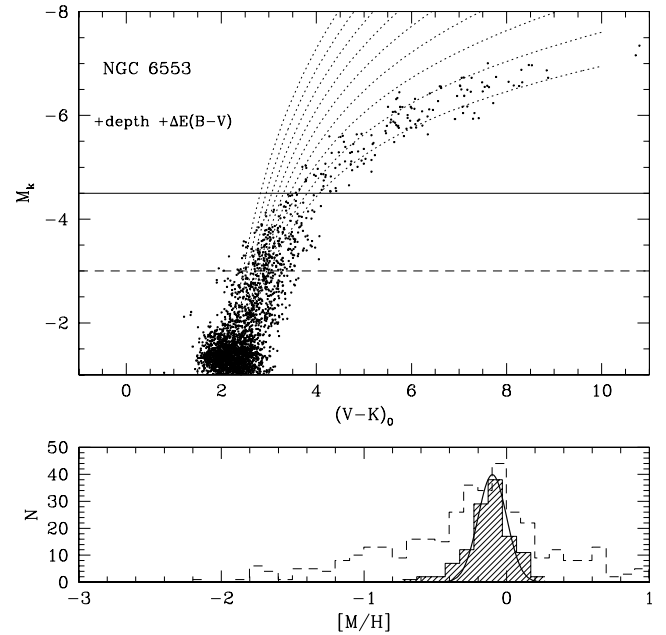


Fig. 11. Upper panel: the CMD of the globular cluster NGC 6553 with overplotted the analytical RGB templates. The dispersion in distance typical of the bulge field at $b = -6^\circ$ and a reddening dispersion of $\Delta E(B - V) = 0.3$ have been added to the cluster CMD in order to simulate the observational biases affecting the derived bulge MD. Lower panel: MD obtained for NGC 6553. Shaded histogram is the MD obtained if only the stars brighter than $M_K = -4.5$ are considered. This MD is well represented by a Gaussian centered in $[M/H] = -0.1$ and $\sigma = 0.1$.

tector (Ferraro et al. 2000); perhaps the use of a more modern instrument may clarify the issue.

As evident from Figure 10, the sensitivity to metallicity is a strong function of the position in the CMD, hence of metallicity itself. The leverage increases with both luminosity and color, being favored at high metallicities by the increasing TiO blanketing in the V band causing redder and redder $V - K$ colors.

In order to investigate the effect of distance and reddening dispersion on the MD derived using the adopted method we simulated such effects on the $(M_K, V - K)$ CMD of the bulge cluster NGC 6553 (Guarnieri et al. 1998). To each star of NGC 6553 we associated a distance modulus randomly extracted according to a bulge space density distribution of the form $\rho = \text{Const} \times r^{-3.7}$ (Sellwood & Sanders 1988; Terndrup 1988), where r is the spatial distance from the Galactic center. The line of sight integration at the field position $((l, b) = (0, -6))$ gives a $1-\sigma$ dispersion of 0.13 mag in the distance modulus, the distribution being close to Gaussian in the core, but with somewhat broader wings. A top hat reddening distribution of ± 0.15 was also adopted. The latter is believed to be an upper limit to the observed bulge reddening variation across our field, but has been chosen as a conserva-

tive assumption, in order to have an upper limit on the possible biases in the derived MD. Random extractions of both distance modulus and reddening were repeated 6 times for each star in the original CMD by Guarnieri et al. (1998) in order to obtain a more populated CMD. Figure 11 shows the resulting simulated CMD including distance and reddening dispersion effects (upper panel). The lower panel shows the MD obtained in the same way as that to be applied to the bulge, and reveals two interesting effects. First, if all the stars brighter than $M_K = -3$ are considered, the resulting MD (dashed histogram) is extremely broad with a long metal-poor tail. This is entirely due to the fact mentioned above: the separation between the RGBs corresponding to different metallicities becomes very small towards faint magnitudes, much smaller than the magnitude/color dispersion due to distance and reddening dispersions. However, if the analysis is restricted to stars brighter than $M_K = -4.5$ then the derived MD shows a fairly sharp peak at $[M/H] = -0.1$ (i.e., centered on the adopted metallicity for this cluster), well fitted by a Gaussian distribution with $\sigma = 0.1$ (FWHM=0.24). This exercise demonstrates that, as long as the analysis is confined to the stars brighter than $M_K = -4.5$: *i*) one should not expect systematic biases; *ii*) the spread introduced by the distance and reddening dispersions is of the order of ~ 0.1 dex in $[M/H]$; and *iii*) contamination by AGB stars (which would introduce a bias artificially skewing the distribution towards the metal-poor side) is negligible at these magnitudes due to the exclusion of the more populated (and bluer) AGB “clump”, located at $M_K \sim -3$. We therefore restrict to $M_K < -4.5$ the derivation of the bulge MD.

4.2. The Resulting Metallicity Distribution

Figure 12 shows the analytical RGBs overplotted to the bulge upper RGB. The dotted part of each RGB is the extrapolation above the theoretical location of the RGB tip (c.f., Section 7), hence only AGB stars are expected in this region. The metallicities of the analytical RGBs range from $[M/H] = +0.2$ to -1.8 , in steps of 0.2. Note that the most metal-rich templates have metallicity of $[M/H] = -0.1$, therefore the shape of the analytical RGBs for higher metallicity is the result of a small extrapolation. Stars bluer than $V - K = 2.8$ (vertical dashed line) were not considered, in order to exclude a few bluer objects that are most likely a disk residue due to imperfect statistical decontamination. Stars fainter than $M_K = -4.5$ (horizontal dashed line) were excluded as well, for the reasons explained above. After these cuts, a sample of 503 stars has been used to derive the bulge MD. It is already clear from this figure that most of the bulge stars are located between the $[M/H] \simeq 0.1$ and $[M/H] = -0.6$ templates, with a peak at $[M/H] = -0.1$ and very few stars more metal-poor than ~ -1 . Formally, super-solar metallicity stars ($[M/H] > 0$) represent 29% of the sample. This should be regarded as an upper limit, due to the *diffusion* to higher $[M/H]$ values

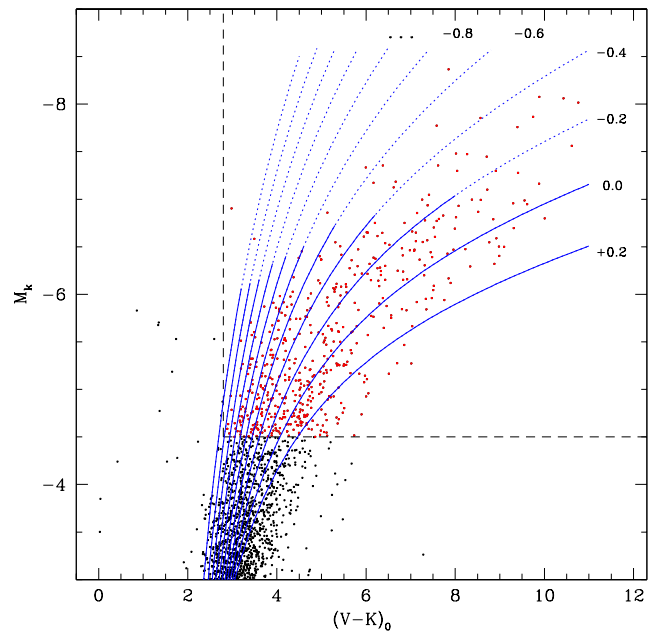


Fig. 12. The bulge V, K CMD compared with the analytical RGB templates. The adopted bulge distance modulus is $(m - M)_0 = 14.47$ while the mean reddening is $E(B - V) = 0.45$. Only the stars inside the dashed box where used for the MD determination.

caused by the dispersion in distance, reddening, etc. (see Fig. 11).

Before proceeding to derive the bulge MD a few biases must be quantitatively evaluated and compensated for: 1) the rate at which stars leave the main sequence (called *evolutionary flux* in Renzini & Buzzoni 1986) has a slight metallicity dependence, 2) the rate of evolution along the RGB scales as $Z^{-0.04}$ (Rood 1972), and 3) by adopting the $M_K = -4.5$ cut one samples (bolometrically) deeper on the RGB the higher the metallicities.

The amplitude of these factors is shown in Fig. 13. The upper panel shows how the evolutionary flux changes as a function on metallicity, relative to its value at Z_\odot . The middle panel shows the combination of effect 2) and 3) mentioned above: the time spent on the RGB, from $M_K = -4.5$ to the tip, normalized at solar value, slowly increases as a function of metallicity. Finally the lower panel shows the combination of the two factors above, which is the correction to apply to each metallicity bin of the MD to take into account the evolutionary effects. Since the evolutionary flux and the RGB lifetime have opposite behaviour with metallicity, the final correction factor is never larger than few percent, well within the intrinsic precision of our measurement.

The resulting bulge MD for the 503 stars in Fig. 12 is finally shown in the three panels of Fig. 14 as a shaded histogram. Also shown in Fig. 14, as thick “open” histograms, are the bulge MDs determined from various spectroscopic studies, normalized to the total number of stars in our

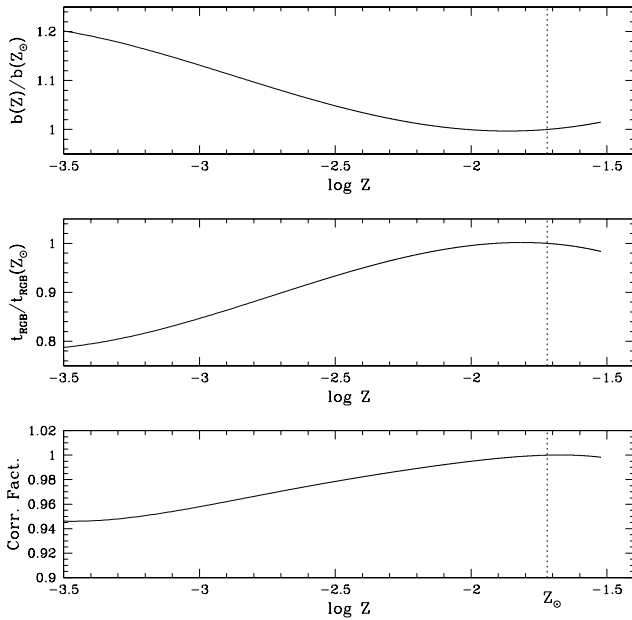


Fig. 13. Upper panel: the ratio of the evolutionary flux at any Z to the same quantity at solar Z . Middle panel: the time spent on the RGB from $M_K = -4.5$ to the tip, with respect to the value at Z_\odot . Lower panel: the product of the two factors above, i.e., the correction factor that one should apply to the MD found from the CMD, in order to take into account these effects.

sample. Note that all these spectroscopic determinations of the bulge MD refer to $[\text{Fe}/\text{H}]$ abundance. Since the template RGBs are on the $[\text{M}/\text{H}]$ scale, we subtracted from the bulge $[\text{M}/\text{H}]$ distribution the same α -element enhancement (i.e., 0.2 for $[\text{Fe}/\text{H}] > -1$ and 0.3 for $[\text{Fe}/\text{H}] < -1$) that had been applied to the template GCs, in order to obtain a $[\text{Fe}/\text{H}]$ distribution. Although the bulge high resolution studies do not permit to draw strong conclusions on the α -element enhancement, the similarity of the bulge CMD with that of bulge GCs would favor a similar chemical enrichment history. Certainly the new generation multi-object spectrographs will allow us to improve our knowledge in this field.

The comparisons shown in Fig. 14 shows that the present, “photometric” MD is broadly consistent with the spectroscopic ones by McWilliam & Rich (1994) and Ramirez et al. (2000), with just a somewhat less pronounced supersolar $[\text{Fe}/\text{H}]$ tail in the photometric MD. (This characteristic is exacerbated in the comparison with the MD of Sadler et al. (1996), based on low resolution data.) We caution, however, that the position of the high $[\text{Fe}/\text{H}]$ cutoff is entirely dependent on the metallicity assigned to the two template clusters NGC 6528 and NGC 6553. For instance, the apparent discrepancy with, e.g., McWilliam & Rich (1994) at high metallicity would disappear if we would have assigned to NGC 6528 and NGC 6553 a metallicity ~ 0.2 dex higher. Indeed this

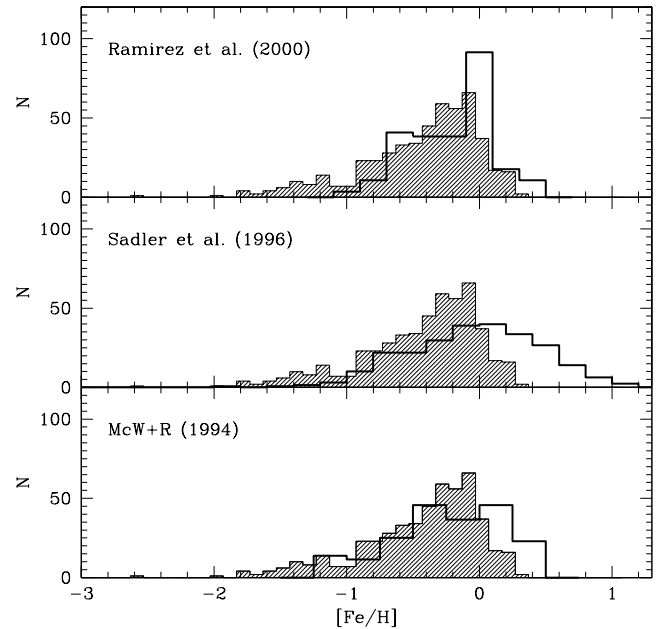


Fig. 14. Comparison between the bulge MD derived from Fig. 12 (shaded histogram) and those derived with spectroscopic surveys.

would bring to coincidence with M&R the high metallicity cutoff, while stretching the distribution and reducing the excess at $[\text{Fe}/\text{H}] \sim -0.2$. We believe that the homogeneous high-resolution studies of cluster *and* bulge field stars that will soon become available, e.g., with the forthcoming FLAMES multifibre spectrograph on VLT (Pasquini et al. 2000), will clarify this problem.

On the other hand, we tend to consider as quite reliable the sharpness of the cutoff at high $[\text{M}/\text{H}]$. Due to the TiO blanketing in the V band, the $V - K$ color of RGB stars has a strong, rapidly increasing sensitivity to $[\text{M}/\text{H}]$, and any high metallicity tail would have resulted in a dramatic broadening of the upper RGB, which instead is clearly absent in the CMD of the bulge shown in Fig. 9. Moreover, the high $[\text{Fe}/\text{H}]$ cutoff would be even sharper, had we underestimated the effect of the distance and reddening dispersions.

4.3. Inferences for the Chemical Evolution of the Bulge

The most straightforward approach is now to compare this empirical MD with the Simple (or one-zone, closed-box) Model of chemical evolution (Searle & Sargent 1972). Rich (1990) first made this comparison for the bulge and found the Simple Model to be a good fit to the abundance distribution from Rich (1988). The Simple Model assumes that no infall or outflow of metals has occurred during the star-forming phase of the system. The distribution follows the relation $N(Z) = y^{-1} \exp^{-Z/y}$, where the single parameter y , the yield, is given by $y = \langle Z \rangle$. Hence, the yield is the average metallicity of the stars in a one-zone system fol-

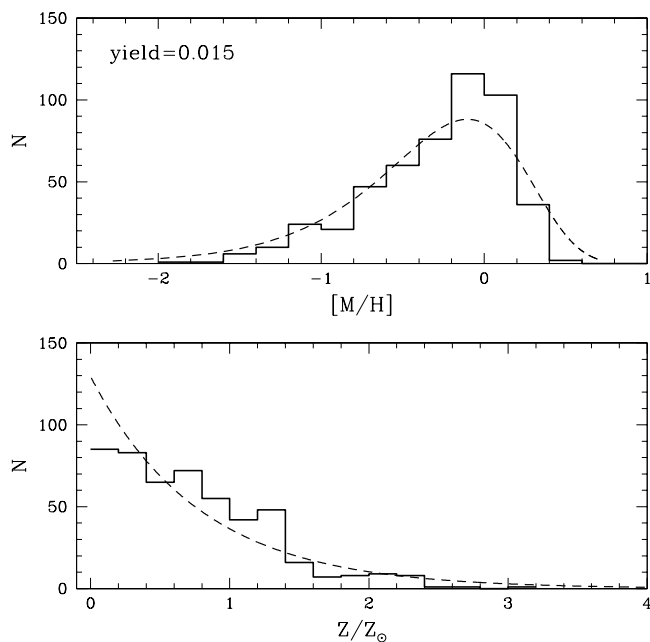


Fig. 15. Comparison between the metallicity distribution of bulge giants from the present study (histogram) and the prediction of the Simple Model (*closed-box* model) with the indicated value of the yield ($y \equiv \langle Z \rangle$). The model distribution has been scaled by the total area under the data histogram. There is a clear shortage of stars near zero metallicity, and an excess of stars near solar abundance, but the one-zone model appears to fit the abundance distribution reasonably well.

lowing the exhaustion of the gas (Hartwick 1976; Mould 1984). If metals are lost from the system by outflow, the functional form of the distribution is unchanged, but the mean abundance $\langle Z \rangle$ is the yield (as would be calculated from supernova models) reduced by the appropriate outflow parameter.

Fig. 15 shows a plot of the Simple Model distribution (for $y = \langle Z \rangle = 0.015$) overlaying the data. Note that both panels show the same model and the same data, once using $[M/H]$ and once using Z/Z_{\odot} as abscissa. As the Simple Model satisfies the requirements of a probability distribution, the function is scaled by the area under the data histogram, so that the area covered by data and fit are identical.

From the plots, the general shape of the abundance distribution is in fairly good agreement with the Simple Model. However, there are noticeable deviations: in the subsolar regime ($Z < 0.3 Z_{\odot}$) less stars are observed than predicted, while with respect to the model there is an excess of near-solar metallicity objects. This excess can be traced back to the fairly sharp clustering of the bulge stars around the RGB template at such metallicity (see again Fig. 7 and 10). This feature is most likely real, as many factors conjure to broaden the derived distribution (dispersion along the line of sight, differential reddening,

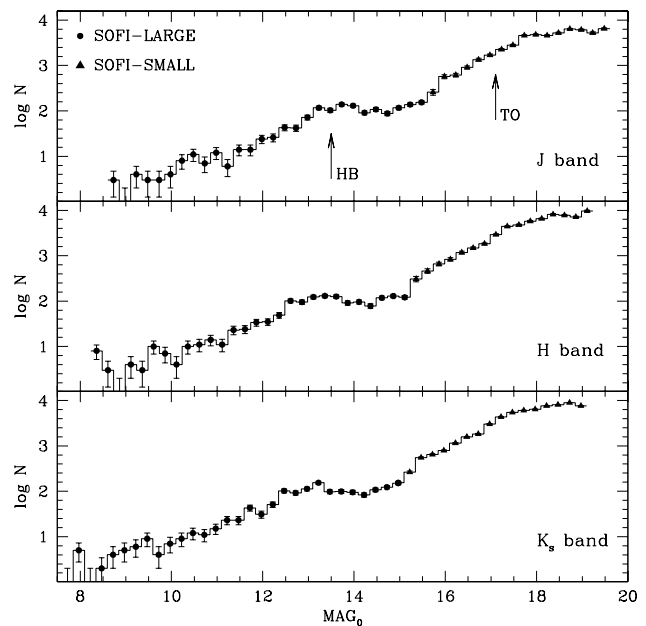


Fig. 16. The bulge near-IR LF as obtained from the SOFI data.

incomplete disk decontamination, etc.). For the same reasons, most likely real is the sharp cutoff at high metallicity, that may even be sharper given the mentioned effects that tend to smooth out any sharp feature in the MD. The moderate shortage of metal-poor stars compared to the Simple Model may flag the presence of a *G-dwarf* problem, a point on which we return in Section 8.

The sharp high-metallicity cutoff of the MD suggests that star formation did not proceed to complete gas consumption. If the bulge formed in a rapid and intense starburst, one can imagine that much of the metals would have been produced *in situ* in core-collapse supernovae, eventually driving strong, metal-rich galactic winds. There are at least two independent arguments favoring this scenario, one direct and one indirect: a) high redshift galaxies thought to be proto-bulges are observed to have strong metal enriched winds (Steidel et al. 1996), and b) in clusters of galaxies at least as much metal mass is out of galaxies in the intracluster medium, as there is locked into stars inside galaxies, which is taken as evidence for early metal-enriched galactic winds (Renzini 1997, 2002). Therefore, a relatively sharp cutoff at the metal rich end, such as we observe, would result if the star formation was sufficiently violent as to eventually evacuate the gas from the proto-bulge before it was exhausted by star formation.

5. The Luminosity Function of the Bulge

The disk-decontaminated CMD shown in Fig. 5c has been used to construct the bulge luminosity function (LF) from the RGB tip down to ~ 1 mag below the main sequence turnoff, in each of the three bands: *J*, *H* and *K_s*, with the results being shown in Fig. 16. The number counts in

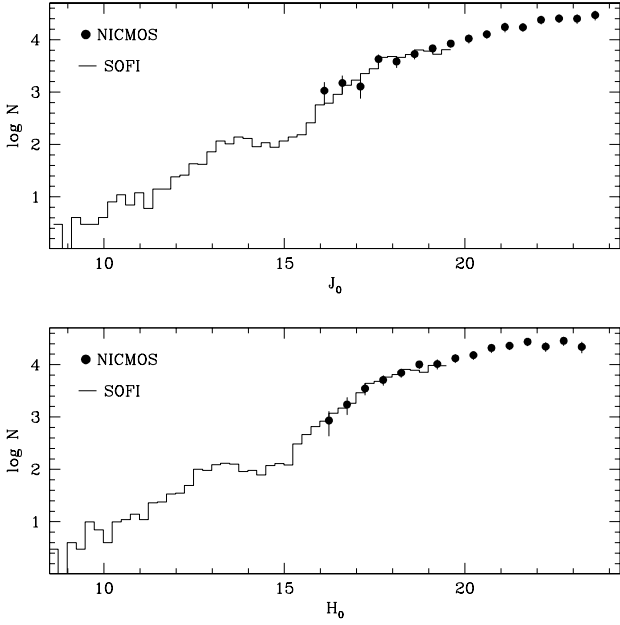


Fig. 17. The bulge LF from this work complemented with the one obtained in Paper II from NICMOS data.

the SOFI-SMALL field ($J > 16$, $J_0 > 15.61$) have been normalized to those in the SOFI-LARGE field, according to the ratio of their areas.

For an easier comparison with the LFs of other objects, or different bulge regions, the LFs presented here are always shown as a function of dereddened magnitude. The adopted average $E(B-V)$ is 0.45, as derived from the comparison with the fiducial loci of the CMD of NGC 6528 (Fig. 9). The relations between the absorptions in different bands have been assumed to be $A_V = 3.1 \times E(B-V)$, $A_I = 0.479 \times A_V$, $A_J = 0.282 \times A_V$, $A_H = 0.190 \times A_V$, and $A_K = 0.114 \times A_V$ (Cardelli et al. 1989).

The broad peak at $J_0 \sim 13.2$ in Fig. 16 is the HB clump, slightly “bimodal” because merged with the RGB bump, as already discussed in Section 4. The main sequence turnoff is located at $J_0 = 17.05 \pm 0.20$, as determined from Fig. 5. The steep decrease in the number of stars that could be expected just above the turnoff, is in fact smeared in this LF due to depth effect, differential reddening, metallicity dispersion, photometric errors and blending effects (see below).

Figure 17 shows the comparison, in J and H , between the SOFI LF and the very deep NICMOS LF from Paper II. A simple normalization by the ratio of the field areas brings the NICMOS LF in perfect agreement with the SOFI one, based on a field more than 100 times larger. Note that the disk contribution to the NICMOS LF was subtracted using Kent (1992) model LF of disk and bulge (cf., Paper II for details).

The upper panel of Fig. 18 shows the comparison between the SOFI LF and the LF by Tiede, Frogel & Terndrup (1995; TFT) in the same bulge region, but on

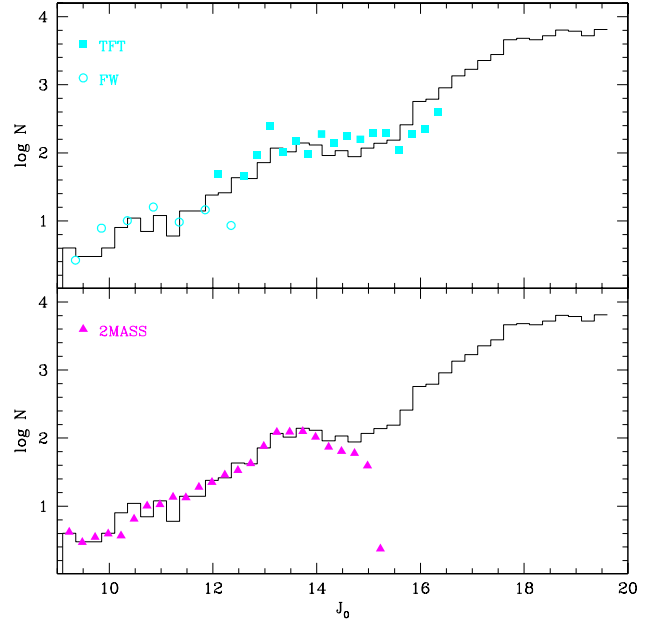


Fig. 18. Comparison with previously published bulge LFs. Counts from different sources have been scaled according to the ratios of the field area and to the different surface brightness, if referring to another bulge region. Histogram: this work; filled squares: data from Tiede, Frogel & Terndrup (1995); open circles, data from Frogel & Whitford (1987); filled triangles: data from the 2MASS sky survey.

a smaller area (4056 arcsec²). The disk contribution has been subtracted from the TFT star counts using the ratio between bulge and disk stars computed from Fig. 5a,b. The upper panel of Fig. 18 also shows the LF obtained by Frogel & Whitford (1987; FW in the figure label) for the M giants in Baade’s Window. The latter has been normalized both for the different area and the surface brightness difference between the two fields.

The lower panel of Fig. 18 shows the comparison with the counts from the 2MASS survey, also normalized only for the ratio of the field areas. The 2MASS counts plotted here were extracted from a region of 927 arcmin², centered on the SOFI field. In the range where they are complete, i.e., for $J_0 < 15$ the 2MASS counts agree perfectly well with the SOFI counts, and are consistent with TFT and FW counts.

Finally, Fig. 19 shows the comparison with the K -band bulge LF from DePoy et al. (1993). The latter was obtained from the photometry of a 604 square arcmin fields towards Baade’s Window, and included disk stars. The two LF were normalized according to the different field area and surface brightness, and the foreground disk contamination, estimated from the present data, has been subtracted from the Depoy LF.

From the combination of the data from 2MASS, SOFI, and NICMOS, a composite LF for the Galactic bulge can

Table 3. Complete near-IR bulge luminosity function^a

J_0	$\log N_J$	H_0	$\log N_H$	K_0	$\log N_K$
7.98	-0.242	7.61	0.117	7.27	-0.008
8.23	-0.184	7.86	-0.008	7.52	0.168
8.48	-0.485	8.11	0.144	7.77	0.256
8.73	-0.133	8.36	0.293	8.02	0.418
8.98	0.027	8.61	0.504	8.27	0.469
9.23	0.621	8.86	0.526	8.52	0.418
9.48	0.469	9.11	0.536	8.77	0.481
9.73	0.547	9.36	0.594	9.02	0.557
9.98	0.594	9.61	0.805	9.27	0.776
10.23	0.566	9.86	0.794	9.52	0.800
10.48	0.811	10.11	0.962	9.77	0.904
10.73	1.007	10.36	1.062	10.02	0.926
10.98	1.027	10.61	1.138	10.27	1.144
11.23	1.136	10.86	1.149	10.52	1.095
11.48	1.128	11.11	1.210	10.77	1.260
11.73	1.279	11.36	1.352	11.02	1.250
<u>11.98</u>	<u>1.352</u>	<u>11.61</u>	<u>1.383</u>	<u>11.27</u>	<u>1.428</u>
12.23	1.415	11.86	1.447	11.52	1.416
12.48	1.633	12.11	1.553	11.77	1.500
12.73	1.623	12.36	1.733	12.02	1.568
12.98	1.857	12.61	2.003	12.27	1.784
13.23	2.068	<u>12.86</u>	<u>2.075</u>	12.52	2.006
13.48	2.013	13.11	2.090	<u>12.77</u>	<u>2.085</u>
13.73	2.143	13.36	2.114	13.02	2.121
13.98	2.114	13.61	2.100	13.27	2.188
14.23	1.959	13.86	1.959	13.52	1.991
14.48	2.033	14.11	1.982	13.77	1.996
14.73	1.944	14.36	1.892	14.02	1.978
14.98	2.068	14.61	2.072	14.27	1.919
15.23	2.140	14.86	2.111	14.52	2.033
15.48	2.188	15.11	2.083	14.77	2.090
15.73	2.412	15.36	2.487	15.02	2.179
15.98	2.756	15.61	2.665	15.02	2.187
16.23	2.790	15.86	2.818	15.27	2.422
16.48	2.957	16.11	2.918	15.52	2.740
16.73	3.130	16.36	3.071	15.77	2.813
16.98	3.228	<u>16.61</u>	<u>3.191</u>	16.02	2.916
<u>17.23</u>	<u>3.376</u>	<u>16.86</u>	<u>3.320</u>	16.27	3.080
17.48	3.518	17.11	3.478	16.52	3.218
17.73	3.666	17.36	3.598	16.77	3.285
17.98	3.612	17.61	3.676	17.02	3.504
18.23	3.591	17.86	3.737	17.27	3.661
18.48	3.676	18.11	3.803	17.52	3.760
18.73	3.764	18.36	3.890	17.77	3.802
18.98	3.814	18.61	3.977	18.02	3.826
19.23	3.854	18.86	4.013	18.27	3.904
19.48	3.901	19.11	4.008	18.52	3.926
19.73	3.952	19.36	4.033	18.77	3.971
19.98	4.001	19.61	4.094	<u>19.02</u>	<u>3.903</u>
20.23	4.039	19.86	4.138		
20.48	4.075	20.11	4.162		
20.73	4.141	20.36	4.213		
20.98	4.219	20.61	4.290		
21.23	4.246	20.86	4.335		
21.48	4.232	21.11	4.348		
21.73	4.262	21.36	4.385		
21.98	4.343	21.61	4.433		
22.23	4.400	21.86	4.417		
22.48	4.410	22.11	4.356		
22.73	4.401	22.36	4.361		
22.98	4.397	22.61	4.432		
23.23	4.413	22.86	4.452		
23.48	4.449	23.11	4.386		
23.73	4.492	23.36	4.290		
23.98	4.535				

^a Horizontal lines mark the boundaries between 2MASS, SOFI and NICMOS based data, from top to bottom.

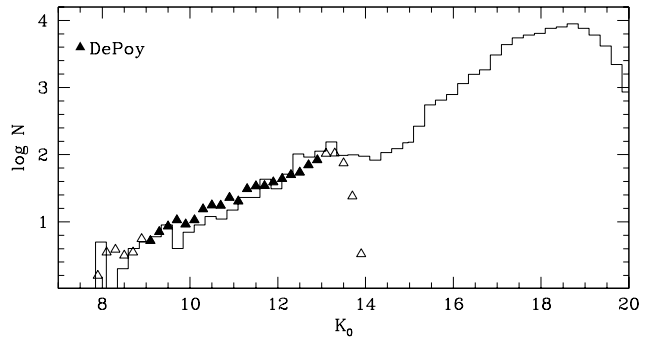


Fig. 19. Comparison with the K -band LF by DePoy et al. (1993). Open symbols refer to counts affected by incompleteness at the faint end and by saturation at the bright end.

be constructed, using the best data for each luminosity range. The result is reported in Table 3, that lists the star counts for J , H , and K_s bands, while Table ?? lists the optical V and I LF. Note that NICMOS data are available only in the J and H bands. All the counts have been normalized to the area of $8'3 \times 8'3$ mapped by the SOFI-LARGE field: i.e., the 2MASS counts have been divided by 13.43, the SOFI-SMALL counts have been multiplied by 4.6, and the NICMOS counts have been multiplied by 609. These scaling factors can be used to calculate the Poissonian errors associated with the counts in each bin. The numbers in Table 3 have been corrected for both disk contamination and incompleteness, although the latter is only significant for the few faintest bins of the NICMOS LF, and it is always $\lesssim 50\%$.

5.1. Simulated CMD and Theoretical LF

In order to compare our observations to corresponding theoretical predictions we have developed a simulator which generates the CMD of a stellar population with a single age and a wide metallicity spread. In this way, we neglect the presence of an age spread, which is justified since the location of the RGBs of (relatively) old stellar populations is much more sensitive to metallicity than to age. The code results from a development of the CMD simulator used in Greggio et al. (1998), adapted to describe single age Stellar Populations with a wide metallicity spread. A thorough description of it can be found in Rejkuba (2002, PhD thesis). We give here a short report, and specify the ingredients used in our simulations.

A Monte Carlo procedure is used to extract mass and metallicity of a simulated star, which gets then positioned on the H-R diagram via interpolation among isochrones. The determined bolometric magnitude and effective temperature are transformed into monochromatic magnitudes by interpolating within bolometric correction tables. Incompleteness and photometric errors, as measured on the real frames are applied. In particular this includes the brightening effect due to blending that was

Table 4. Optical bulge luminosity function.

V_0	$\log N_V$	I_0	$\log N_I$
11.73	-1.110	10.46	-0.381
11.98	-1.106	10.71	-0.038
12.23	-0.406	10.96	0.501
12.48	0.010	11.21	0.646
12.73	0.345	11.46	0.773
12.98	0.663	11.71	0.918
13.23	0.910	11.96	1.072
13.48	1.024	12.21	1.153
13.73	1.204	12.46	1.269
13.98	1.370	12.71	1.252
14.23	1.552	12.96	1.402
14.48	1.707	13.21	1.498
14.73	1.855	13.46	1.559
14.98	2.079	13.71	1.685
15.23	2.138	13.96	1.950
15.48	2.089	14.21	2.143
15.73	2.058	14.46	2.087
15.98	2.133	14.71	2.090
16.23	2.130	14.96	1.953
16.48	2.119	15.21	1.864
16.73	2.240	15.46	2.001
16.98	2.346	15.71	2.036
17.23	2.467	15.96	2.119
17.48	2.718	16.21	2.213
17.73	2.906	16.46	2.368
17.98	3.126	16.71	2.480
18.23	3.232	16.96	2.685
18.48	3.334	17.21	2.937
18.73	3.398	17.46	3.122
18.98	3.408	17.71	3.226
19.23	3.457	17.96	3.371
19.48	3.453	18.21	3.414
19.73	3.454	18.46	3.500
19.98	3.475	18.71	3.529
20.23	3.477	18.96	3.542
20.48	3.466	19.21	3.583
20.73	3.462	19.46	3.606
20.98	3.436	19.71	3.601
21.23	3.457	19.96	3.611
21.48	3.422	20.21	3.654
21.73	3.422	20.46	3.609
21.98	3.456	20.71	3.614
22.23	3.400	20.96	3.417
22.48	3.359	21.21	3.287

discussed in Section 2.1. The procedure is iterated until the number of objects observed in some CMD region is reached.

The isochrones data base consists of Cassisi and Salaris (1997) models, implemented with Bono et al. (1997), plus some additional models explicitly computed for this application with the code described in Cassisi and Salaris (1997) and Cassisi, Salaris and Bono (2002). The metallicity range goes from $Z=0.0001$ to $Z=0.04$, and the helium abundance varies in locksteps with Z following $Y \simeq 0.23 + 2.5Z$.

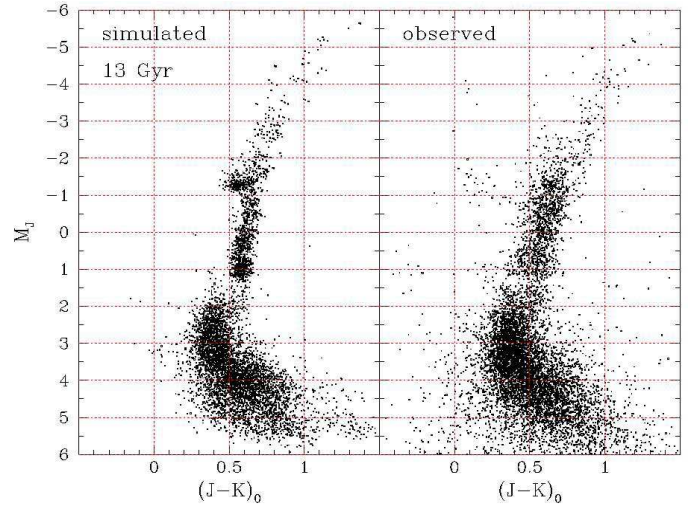


Fig. 20. Left panel: simulated CMD for a 13 Gyr old population with the MD determined in Section 4. Right panel: the bulge CMD for the SOFI-LARGE field.

Theoretical bolometric corrections (BCs) have been obtained by convolving the model atmospheres computed by Castelli et al. (1997) with the Landolt V and I and the SOFI J, H, K_s filter passbands and fixing the zero point such that $BC_V = -0.07$ for the model of the Sun, and all the colors are zero for the model of Vega. However, the brightest stars in our sample are cooler than $T \sim 4000\text{K}$, limit below which current model atmospheres are known to fail to reproduce the observed spectra, due to the inappropriate treatment of molecules. Therefore, the empirical BCs by Montegriffo et al. (1998) were used instead of the theoretical ones for temperatures $T \lesssim 4000\text{K}$. The dependence of the BCs on the metallicity parameter is taken into account in the simulations.

The results of the artificial stars experiments described in Section 2 have been used to assign the detection probability and the photometric error (i.e. the difference between input and output magnitude) to the simulated stars. The synthetic CMD has thus the same observational biases as that obtained from the measured frames.

A number of simulations have been computed for ages ranging from 8 to 15 Gyr, and by adopting:

- i*) an IMF slope of -1.33 , as found in Paper II
- ii*) the metallicity distribution derived in Section 4
- iii*) an average distance modulus of $(m - M)_0 = 14.47$ and reddening of $E(B - V) = 0.42^4$. Each obtained synthetic CMD has been further dispersed for depth ($(\rho(r) \propto r^{-3.7})$ and variable reddening ($\Delta E(B - V) = \pm 0.15$) effects.

Figure 20 (left panel) shows the synthetic CMD for a 13 Gyr old population with the characteristics described

⁴ This value is 0.03 magnitudes smaller than the one adopted in Section 4, which was derived from the comparison of the mean locus of the $(M_V, V - K)$ bulge CMD with that of NGC 6528. The lower value of $E(B - V) = 0.42$ is instead required for a best fit with the adopted isochrones, and therefore for a consistent comparison with the synthetic CMD.

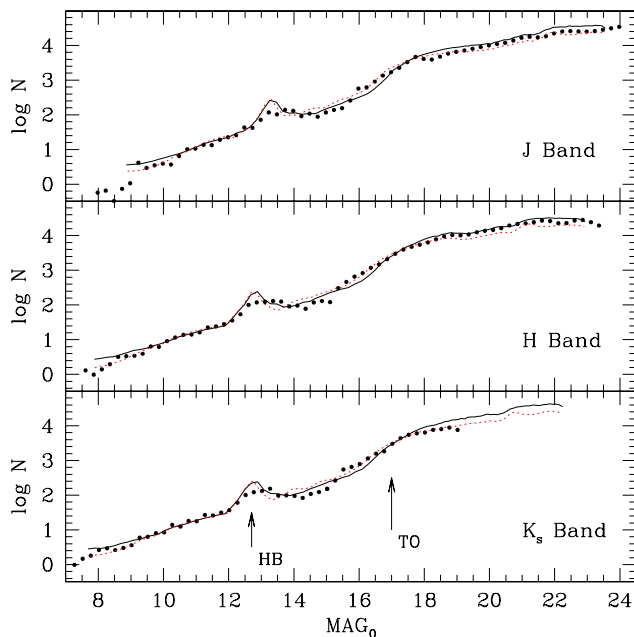


Fig. 21. The complete bulge LF in the three near-IR bands (dots), as resulting from the combination of the 2MASS, SOFI and NICMOS data (from Table 3). A theoretical LF for an age of 13 Gyr (solid line) and 8 Gyr (dotted line) is shown as a solid line for comparison.

above, and a comparison with the bulge near-IR CMD observed with SOFI is shown in the right panel.

The simulation code was run until the number of stars with $M_J < 1.2$ reached the number of stars sampled by SOFI-LARGE in this CMD region. Then it was run again until extracting as many stars with $M_J > 1.2$ as in the SOFI-SMALL field.

The main purpose of the comparison in Fig. 20 is to show how much the simulation code is able to reproduce the observed CMD, including the observational biases introduced by the dispersions in distance, reddening and metallicity, as well as blending.

Figure 20 shows that indeed the main features of the observed CMD are well reproduced by the simulator. Noticeable exceptions are the morphology of the HB clump, and of the lower RGB. In fact, the observed HB is significantly less defined than the simulated one, and also the color width of the RGB is underestimated by about a factor of two in $J - K$. In principle, this mismatch can be caused by several effect, although none of them, alone, seems convincing to us. Larger spread in the observed CMD can be due to an underestimate of one of the following effects:

i) Distance spread: the bulge density law could be *flatter* than $\rho \propto r^{-3.7}$, and/or the bulge being a bar may increase the distance dispersion along the line of sight. Note that adopting a larger distance dispersion would smear the HB clump, making it more similar to the observed one,

but would not have any appreciable effect on the spread in color of the RGB. Hence, a larger distance spread alone would not be sufficient to make the simulated CMD identical to the observed one.

ii) Differential reddening. Larger values of this parameter would broaden the RGB of the simulated CMD, but also would cause the HB to appear tilted along the reddening line, which is not seen in the observed CMD of the bulge, while it is prominent in e.g., NGC 6553 (Zoccali et al. 2001a). Also, the differential reddening needed to account for the spread in color seen in the near-IR CMD would imply a too large spread in the optical CMD. An attempt was made to correct for differential reddening following the method used for NGC 6553 (Zoccali et al. 2001a), but failed due to the small scale of the reddening variations across the field. Indeed, in the case of NGC 6553, one finds reddening variations of the order of $\delta E(V - I) \sim 0.1$ on scales of only $\sim 20''$.

iii) Photometric errors. Larger SOFI-LARGE photometric errors than adopted in the simulation would certainly help smearing the simulated RGB and HB respectively in color and magnitude, but can hardly solve both problems at once. To smear enough the simulated HB the photometric error should be $\sim 0.3 - 0.4$ mag, which would produce a too broad RGB compared to the observed CMD (see Fig. 20).

iv) Problems in the theoretical models. The RGB temperatures (hence colors) are strongly dependent on the mixing-length parameter, which needs to be empirically calibrated, and there are no perfect calibrators. The models used in the present simulations were calibrated by fitting the RGB of template globular clusters from Frogel et al. (1983) for $[\text{Fe}/\text{H}] \lesssim -0.7$, and at solar metallicity by demanding to the solar model to have the solar radius. Ideally, it would have been preferable to have a homogeneous calibration over the whole metallicity range, but the solar metallicity clusters would have introduced in the calibration the uncertainty in their reddening. As a net result, the adopted mixing length is some 10% larger at $[\text{Fe}/\text{H}] = 0$ than at $[\text{Fe}/\text{H}] \lesssim -0.7$, which has the effect of compressing somewhat the relative spacing of the RGBs as a function of metallicity. This effect goes indeed in the direction of reducing the color dispersion in the simulated RGBs. Moreover, the simulation is also affected by the uncertainty in the bolometric corrections and color-temperature transformations. All in all, Salaris, Cassisi & Weiss (2002) estimate an uncertainty of $\sim 0.10 - 0.15$ mag in the range of optical colors spanned by theoretical RGBs, which can also be taken as indicative of the uncertainty in the range of the near-IR colors.

While the origin of the discrepancy of Fig. 20 is still partly unclear, we proceed to the construction of the theoretical LF from the simulated CMD, keeping in mind that the region around the HB and lower RGB is presently not well reproduced by our simulations. The same code with the same inputs was then used to generate a much larger number of stars compared to the simulation shown in Fig. 20, in order to construct a smooth LF from the up-

per RGB down to the limit of the NICMOS photometry and the result is shown in Fig. 21. The simulation includes photometric error and blending effects, and is meant to match the observed LF after correction for incompleteness.

Figure 21 finally shows the comparison between the observed J, H, K_s LFs (dots) and the theoretical LFs generated from the simulated CMD described above (lines). The observed LFs result from the combination of all the available data, namely 2MASS + SOFI + NICMOS all scaled to the SOFI-LARGE area, as in Tables 3. The simulated LFs refer to 8 and 13 Gyr old populations. Observed and theoretical LFs were normalized to the total number of stars with $MAG_0 < 12$ in all bands. There is overall agreement between the theoretical and the observed LFs, though the HB clump + RGB bump appears much sharper in the simulation than in the observed LF, as expected from Fig. 20.

This comparison also shows that formally the 8 Gyr isochrone gives a slightly better fit to the data above the turnoff, which is the part of the LF sensitive to age. However, the same effect causing the smearing of the HB would have also made shallower the drop off of the luminosity function just above turnoff, hence making the bulge population to appear younger than it is when comparing to the simulated LFs. Hence, we believe that before having identified the origin of the additional RGB and HB dispersion the comparison of simulated and observed LFs cannot set more stringent constraints on the age of the bulge stars other than being ~ 10 Gyr.

5.2. The Bulge Spectral Energy Distribution

Integrating the LFs in Tables 3 and 4, one can determine the total luminosity of the sampled bulge stellar population in each band. This has been performed using the whole database (NICMOS, SOFI, 2MASS for the infrared and WFI for the optical), then normalizing the results to the area of the SOFI-LARGE field. For the J and H bands the NICMOS data allow to include the contribution of all stars down to $\sim 0.15M_\odot$. The K -band contribution of stars fainter than the SOFI limit has been estimated from the theoretical M/L ratio of lower main sequence stars and adopting -1.33 for the slope of the IMF, and found to be just a fraction $\sim 10^{-5}$ of the total K -band luminosity. This result is not surprising given the flat bulge IMF. For the same reason, we integrated the V and I LFs of Table 4 safely neglecting the contribution of the lower MS stars. The resulting sampled luminosities are:

$$\begin{aligned} L_V &= 1.00 \times 10^5 L_{V,\odot} \\ L_I &= 1.13 \times 10^5 L_{I,\odot} \\ L_J &= 2.84 \times 10^5 L_{J,\odot} \\ L_H &= 3.67 \times 10^5 L_{H,\odot} \\ L_K &= 4.20 \times 10^5 L_{K,\odot}, \end{aligned}$$

where the solar magnitudes have been taken from Allen (2000). To derive monochromatic fluxes, the integrated

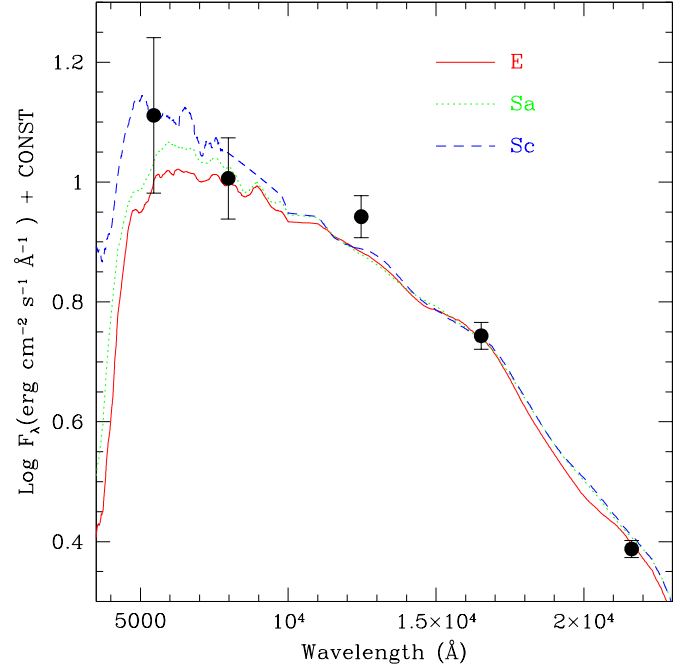


Fig. 22. The spectral energy distribution of the bulge summing the contribution of all individual star (filled circles). The error bars here show what would be the *systematic* displacement of all the points if an uncertainty of $E(B - V) = \pm 0.1$ is allowed. Superimposed are the spectral energy distributions of template galaxies from Mannucci et al. (2001).

magnitudes in each band have been transformed to AB magnitudes, and the monochromatic flux has been calculated as $\log F_\nu = -0.4 m_{AB} + 19.44$ (Oke & Gunn 1983), with $F_\lambda = F_\nu c / \lambda^2$. Figure 22 shows the resulting spectral energy distribution (SED) of the galactic bulge, compared to the template spectra of elliptical, Sa and Sc galaxies from Mannucci et al. (2001). The Galactic bulge follows quite well the Sc template, which is not surprising given that the Milky Way is indeed an Sbc galaxy. For the optical part of the spectrum, the Mannucci et al. templates rely on those by Kinney et al. (1996), which in the case of Sc galaxies come from the integrated spectra of a region $10'' \times 20''$ wide at the center of the two galaxies NGC 2403 and NGC 598, whose radii are 10.6 and 35.2 arcmin respectively, i.e., the sampled regions are located well inside the bulge of these galaxies. Visual inspection of a DSS image of NGC 2403 suggests that the aperture used to derive the spectrum of this galaxy almost certainly includes a few site of active star formation. Their effect is however minimal in the V and I bands, while dominating the spectrum only in the IUE ultraviolet.

On the other hand, the average value of the Mg_2 index of the ellipticals in the Kinney et al. sample is 0.314, which compares to $Mg_2=0.23$ (Puzia et al. 2002) for the Galactic bulge. Hence, our bulge is quite metal poor com-

pared to giant ellipticals, which accounts for its bluer SED. Actually, the computation of the theoretical Mg_2 index for a composite stellar population with the Bulge MD as determined here yields values as low as 0.16 – 0.19 for ages ranging from 10 to 15 Gyr (Maraston et al. 2002). These values, appropriate for simple stellar population with $[Fe/H] \simeq -0.5$, result from the effect of the well populated subsolar metallicity component on the MD (Greggio 1997). At optical wavelengths, this component provides more relative flux than the high Z one, which results in both a lower composite Mg_2 index, and in a bluer SED.

5.3. The Sampled Luminosity-Star Number Connection

The number of stars with mass in the range 0.15 to $1 M_{\odot}$ in the observed SOFI field can be obtained by integrating the bulge IMF with the appropriate scale factor A :

$$N_{\text{PRED}} = A \int_{0.15}^1 M^{-1.33} dM, \quad (6)$$

with $A \propto L_T$ (Renzini 1998), where L_T is the bolometric luminosity sampled by the SOFI field. For given age, the ratio A/L_T is a weak function of both metallicity and IMF. Its dependence on age is relatively stronger, in fact, from the models by Maraston (2002), at $[M/H] = -0.2$ and for IMF slope of -1.33 , A/L_T ranges from 0.82 to 1.1 for an age varying from 10 to 13 Gyr.

The total bolometric luminosity sampled by the SOFI-LARGE field can be obtained applying the appropriate bolometric corrections to individual stars in the sample. To evaluate that, we have run the simulation code to obtain the bolometric and monochromatic luminosities of a stellar population with the observed metallicity distribution, obtaining: $L_T = 1.39L_V = 1.16L_I = 0.70L_J = 0.53L_H = 0.51L_K$ with the coefficients changing by at most 3% when varying the age from 10 to 13 Gyr. No observational errors were applied in this run.

Using the five monochromatic luminosities with the above relation and averaging the results we obtain a total luminosity of $L_T = 177,000L_{\odot}$, hence $N_{\text{PRED}} = 380,000$ and 510,000, respectively for 10 and 13 Gyr. These numbers compare with the $424,000 \pm 81,000$ stars in the SOFI-LARGE field, the error in the latter being dominated by the Poisson noise in the number of objects in the NICMOS field. Predicted and observed numbers are quite consistent (see also Paper I), since these theoretical estimates are expected to be accurate to within $\sim 10\%$.

5.4. The M/L Ratios

Integrating the IMF from 0.15 to $100 M_{\odot}$, and adopting the prescription in Paper II for the mass of the stellar remnants (those above $\sim 1M_{\odot}$) one derives the total stellar mass in the bulge SOFI-LARGE sample. Using the luminosities in the various bands given above, one then determines the corresponding M/L ratios. This gives:

$$M/L_V = 3.67$$

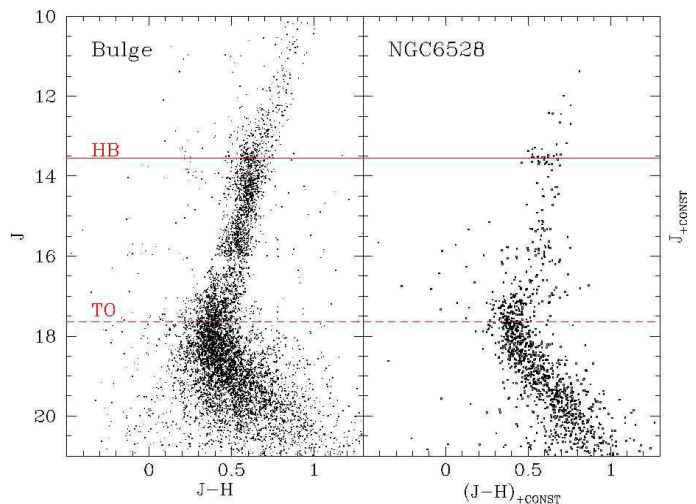


Fig. 23. The bulge and the NGC 6528 CMDs are shown side by side. The magnitude difference between the HB and the turnoff in the bulge CMD (left) is compared with the same quantity for NGC 6528 (right). The CMD for NGC 6528, originally in the NICMOS instrumental ($m_{110}, m_{110} - m_{160}$) plane, has been shifted both in magnitude and in color in order to match the location of the bulge HB.

$$\begin{aligned} M/L_I &= 3.25 \\ M/L_J &= 1.28 \\ M/L_H &= 1.00 \\ M/L_K &= 0.87, \end{aligned}$$

with M/L_K in very nice agreement with the dynamical value, $M/L_K \simeq 1$ (Kent 1992).

6. The Age of the Bulge

Taking advantage of the sharp turnoff region of the decontaminated near-IR CMD derived in Section 3 we proceed to estimate the age of the bulge stellar population. As in paper I, we adopt a differential procedure, comparing the luminosity difference between the HB clump and the MS turnoff of the bulge to that of a globular cluster of similar metallicity.

Fig. 23 shows the comparison between the bulge CMD and that of the cluster NGC 6528, whose metallicity is close to the average of the bulge. The near-IR CMD of NGC 6528 is based on the NICMOS photometry obtained by Ortolani et al. (2001). The magnitude difference between the HB clump and the turnoff is virtually identical in the two diagrams, as emphasized by the two horizontal lines.

This ensures that the difference between the age of the cluster and the *mean* age of the bulge cannot exceed $\sim 20\%$ (thanks to the *rule of thumb* according to which $\delta_{\text{age/age}} \simeq \delta(\Delta M_{\text{TO}}^{\text{HB}})$ (Renzini 1991).

This confirms and reinforces the conclusion in Paper I that the bulk of the bulge population and the clusters

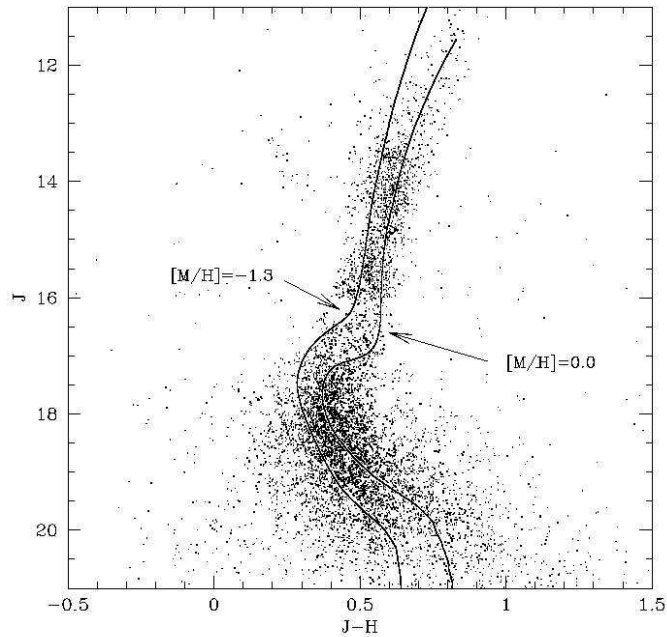


Fig. 24. 10 Gyr isochrones (Cassisi & Salaris 1997) for the two extremes of the bulge MD are overlotted on the CMD.

NGC 6528 and NGC 6553 are coeval. The absence of any appreciable extension of the bulge main sequence beyond the obvious turnoff makes it clear that no trace of an intermediate-age population is detectable in the bulge CMD.

The proper motion decontaminated and differential reddening corrected CMD of NGC 6553 (Zoccali et al. 2001a) and NGC 6528 (Feltzing et al. 2002) confirm the results of Paper I that the HB to TO magnitude difference in these two bulge clusters is virtually identical to that of the inner halo clusters NGC 104 (47 Tuc). Fig. 23 now shows that this magnitude difference is essentially identical also for the bulge field population, strengthening the case for the bulk of the whole population of the Galactic spheroid (i.e. bulge and halo) being essentially coeval, though an age difference of $\sim 20\%$ ($\sim 2 - 3$ Gyr) either way cannot be excluded.

One aspect of the cluster to bulge CMD comparison still deserves some attention. Indeed, the bulge population is affected by dispersion in both distance and metallicity, while the cluster stars are chemically homogeneous and all at the same distance (although affected by some differential reddening). In Fig. 24 two 10 Gyr isochrones spanning the full metallicity range of the bulge are overlotted to the bulge CMD, assuming the same distance and reddening for both of them. This illustrates that the wider dispersion affecting the bulge CMD (compared to the HST/NICMOS CMD of NGC 6528) can be well accounted by the bulge metallicity dispersion, also taking into account the ~ 0.13 mag $1-\sigma$ dispersion due to the distance distribution along the line of sight.

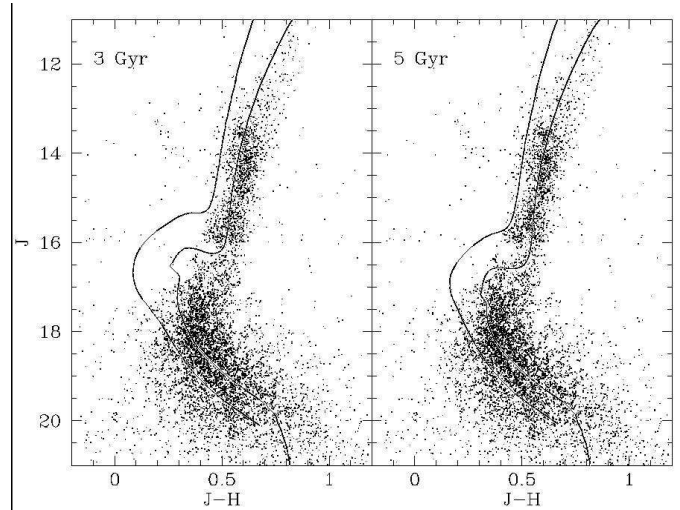


Fig. 25. Comparison of the bulge CMD with two younger isochrones of 3 (left panel) and 5 Gyr (right panel). Two models are plotted in each panel, both referring to the same age. The reddest curve in each panel is for solar metallicity, while the one on the blue side is for $[M/H]=-1.3$.

According to recent attempts at determining the relative ages of Galactic globular clusters the bulk of clusters are coeval within a ± 1.5 Gyr uncertainty, with only the most metal rich ones in the sample appearing to be slightly younger than the others (Rosenberg et al. 1999; Salaris & Weiss 2002). However, these studies do not extend to the high-metallicity clusters of the bulge. For example, Rosenberg et al. assign to 47 Tuc an age 1.2 ± 1.2 Gyr “younger” than that of the bulk of the halo globular clusters. Salaris & Weiss (2002) assign to the same cluster an age of 10.7 ± 1.0 Gyr, compared to 11.7 ± 0.8 Gyr for the prototypical metal poor cluster NGC 7078 (M15). On the other hand, Ortolani et al. (2001) date NGC 6528 at 13 ± 3 Gyr from the value of ΔJ_{TO}^{HB} .

It is clear that, within the uncertainties of the currently available data and dating methods, no appreciable age difference has been unambiguously detected between the bulk of bulge field stars and the globular clusters of either the bulge or the halo. On the other hand, the *absolute* age of the clusters remain more uncertain than the formal error bars sometime quoted by individual authors. Just to mention one example, the age of the globular cluster 47 Tuc has been recently estimated to be 12.5 ± 2 (Carretta et al. 2000), 13 ± 2.5 Gyr (Zoccali et al. 2001b), and 10.7 ± 1.0 Gyr (Salaris & Weiss 2002), the difference being partly due to a difference in the cluster distance and partly to the use of different sets of models.

Significantly younger ages can be excluded, as shown in Fig. 25, where 3 and 5 Gyr isochrones of both solar and $[M/H]=-1.3$ metallicity are overlotted on the bulge CMD. After the submission of this paper, during the refereeing process, we became aware of the paper by Cole & Weinberg (2002), in which the Authors argue that the bulk

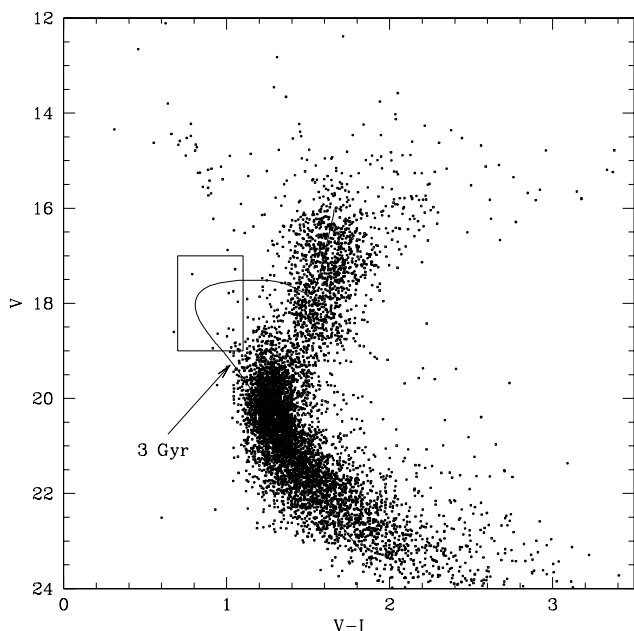


Fig. 26. The disk decontaminated optical CMD, together with the 3 Gyr isochrone for solar metallicity. The box shows the region where the stars of a hypothetical 3 Gyr old “bar” population, spread along the line of sight, would be expected.

of the stellar population of the Galactic “bar” formed less than 6 Gyr ago, with an age of ~ 3 Gyr being favored. As they state “the main sequence turnoff of a 3 Gyr old population should be readily traceable along the Galactic bar from $V \approx 17$ at the near end to $V \approx 19$ at the far end”. Note that the Galactic component called “bar” in Cole & Weinberg (2002) has a mass of $2 \times 10^{10} M_{\odot}$ and therefore is not a minor component, but rather the whole population of the system called here “the bulge”. As evident from Fig. 26, no such intermediate age population is actually detected in the present data.

The region in the CMD just above the main sequence turnoff is so devoid of stars that very few, if any, blue stragglers stars (BSS) may be present in the field (see, e.g., Fig. 24). Among Galactic globular clusters, Ferraro et al. (1995) estimate an average frequency of ~ 1 BSS every $10^3 L_{\odot}$ of bolometric light of the parent cluster, but with very large cluster to cluster variations that are not merely statistical fluctuations. Scaling from the SOFI-LARGE field, the SOFI-SMALL field samples $\sim 177,000/4.6 \simeq 38,000 L_{\odot}$, and one would expect to recover ~ 38 BSSs, if the bulge has the same BSS frequency as the average globular cluster. Clearly it has not. The bulge is far less productive of BSSs than a typical globular cluster, indicative that the cluster environment favors the formation of binaries with the right separation for producing BSSs. Most likely this is due to the dynamical processes that are germane to the clusters.

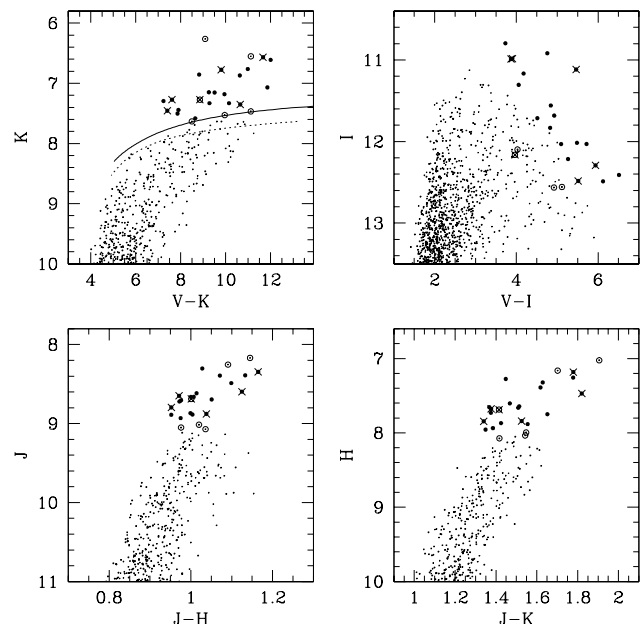


Fig. 27. The bulge RGB tip in different bands. The solid line is the theoretical tip location according to Salaris & Cassisi (1998), while the dashed line is the location of the tip empirically found by Ferraro et al. (2000). Big dots are the (20) stars that lie above the theoretical RGB tip in *all* the bands, while open circles are stars that lie above the tip in *K* but not in *I*. Crosses are blends even in the optical images.

7. The RGB Tip and Above

The tip of the RGB is of special interest for three main reasons: i) any AGB star brighter than the RGB tip is a candidate intermediate age star, hence may signal the presence of an intermediate age population (e.g. Iben & Renzini 1983), ii) the RGB tip itself is directly used as a distance indicator (Lee, Freedman & Madore 1993; Salaris & Cassisi 1997; Sakai, Madore, & Freedman 1999), and iii) in any galaxy the luminosity function near the tip of the RGB has a direct impact on the distance determination using the surface brightness fluctuation method (Tonry & Schneider 1988).

Theoretical models indicate that the bolometric luminosity of the RGB tip (corresponding to the helium flash in the core) increases with metallicity by ~ 0.25 mag per dex (Rood 1972; Sweigart & Gross 1978). However, due to increasing blanketing, in the *I* band the RGB tip magnitude appears to be independent of metallicity for $[\text{Fe}/\text{H}] \lesssim -0.7$, i.e., in the range covered by globular clusters in the Galactic halo (Lee et al. 1993). The present data on the Galactic bulge offer an opportunity to explore the behavior of the RGB tip luminosity at higher metallicities, up to solar and beyond.

Fig. 27a displays the (*K*, $V - K$) diagram of the combined WFI+2MASS field, for the upper RGB+AGB ($K < 10$). Overplotted, as a solid line, is the location

of the theoretical RGB tip for metallicities in the range from $[M/H] = -2.35$ to $[M/H] = -0.28$ (extrapolated here to higher metallicity). For each metallicity, the RGB tip bolometric luminosities from the theoretical models of Salaris & Cassisi (1998) have been converted to K magnitudes and $V - K$ colors using the empirical bolometric corrections from Montegriffo et al. (1998) and the analytical template RGBs described in Section 4. The empirical location of the RGB tip in the template globular clusters is also shown as a dotted line (from Ferraro et al. 2000), with the small offset between the theoretical and empirical RGB tips being probably due to poor statistics near the RGB tip in the template globular clusters.

In Fig. 27, 25 stars lie above the nominal RGB tip in K , and therefore are candidate AGB stars. Three more stars with very red colors ($J - K > 2.5$) lie outside the limits of these plots. Two of them are included in the IRAS catalogue (IRAS18061-3140 and IRAS18069-3153) as OH-IR stars. The third one, missing in our optical CMD due to incompleteness (V mag for the other two stars is 20.7 and 23.7, respectively) is likely to be of the same nature. Two stars in the same CMD region are also present in the disk CMD from 2MASS, therefore suggesting that they are not tracers of a younger bulge population. As well known, in metal poor globular clusters ($[Fe/H] \lesssim -1$) no AGB stars brighter than RGB tip have been found. However, a few stars brighter than the RGB tip do exist in more metal rich globulars, with many of them being long period variables (LPV, Frogel & Elias 1988; Guarneri et al. 1997). The frequency of LPVs in metal rich globulars has been evaluated by Frogel & Whitelock (1998). From their Table 1, one derives an LPV frequency of $\sim 4/(10^6 L_K^\odot)$. The luminosity sampled by the combined WFI-2MASS field is 13.43 times larger than that sampled by the SOF-LARGE field, i.e. $\sim 5.7 \times 10^6 L_K^\odot$, hence one would expect 23 LPVs, while 28 stars are found above the RGB tip. However, an inspection of their optical counterparts in the WFI frames reveals that 6 of them, shown as crosses in Fig. 27, are blended with other dimmer stars, and their intrinsic K -band luminosity will be somewhat dimmer than estimated on 2MASS data. Another 5 stars are definitely below the RGB tip in the optical CMD (Fig. 27b), and are plotted as open circles in the four panels of Fig. 27. Their location may result either from the resolution of 2MASS being much worse (~ 4 arcsec) than that of WFI ($\lesssim 1$ arcsec) and therefore these stars may have unresolved companions in near-IR, that make them artificially brighter. Alternatively they might be LPVs having been caught near minimum light at the time of WFI observations. Finally, our simulations show that ~ 5 RGB stars are expected to be found above the nominal RGB tip due to the depth effect plus differential reddening. On the other hand, other LPVs may have been caught below the RGB, near minimum light. All in all we conclude that the number of stars brighter than the RGB tip is within the expectations as derived from the frequency of LPVs in globular clusters spanning nearly the same metallicity range of the bulge. Of course, not all stars brighter than the RGB tip

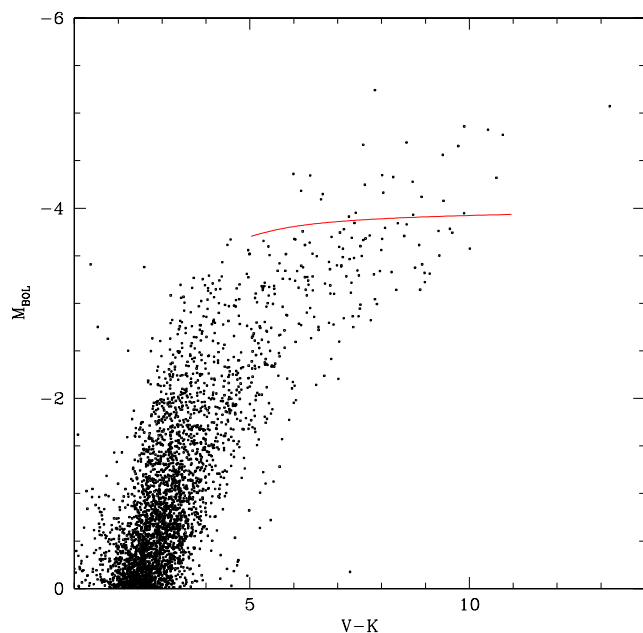


Fig. 28. The absolute bolometric luminosity of upper RGB and AGB stars. The theoretical RGB tip luminosity is also shown as a solid line (the same as in Fig. 27). The bulge AGB stars appear to extend ~ 1 bolometric magnitude above the RGB tip.

in Fig. 27 may be LPVs, hence the present findings do not contradict the result of Frogel & Whitelock (1998), who argue for a deficit of LPVs in the bulge field compared to metal rich globulars. In any event, the bright AGB stars seen in the WFI-2MASS field do not favor the presence of a stellar population in the galactic bulge appreciably younger than the old, metal rich globular clusters, thus reinforcing the conclusion we have drawn from the turnoff region.

The absolute bolometric magnitudes for the stars on the upper RGB and AGB have also been derived using the empirical bolometric corrections from Montegriffo et al. (1998) and the distance and reddening adopted in Section 4. The result is displayed in Fig. 28, showing that the bulge AGB stars extend ~ 1 bolometric magnitude above the RGB tip, reaching $M_{bol} \simeq -5.0$. This is just marginally brighter (by ~ 0.2 magnitudes) than the brightest known LPV member of a metal rich globular cluster, i.e. V4 in NGC 6553 (Guarneri et al. 1997).

Concerning the use of the RGB tip as a standard candle, Fig. 27b shows that the I band magnitude of the tip drops by almost two magnitudes, from the lowest to the highest metallicity spanned by bulge stars. Clearly the I band luminosity of the tip cannot be used as a standard candle above $[Fe/H] \simeq -0.7$. Also in the J band the tip luminosity appears to decrease slightly (Fig. 27c), while it increases slightly in the K band (Fig. 27a). In the H band instead the tip luminosity appears to be fairly constant, suggesting the use of this band for deriving RGB

tip distances of stellar populations in the metallicity range $-1.0 \lesssim [\text{Fe}/\text{H}] \lesssim 0.0$. For even higher metallicities the K band may become more appropriate, as indicated by the theoretical RGB tip luminosity shown in Fig. 27a.

Fig. 27 suggests also quite obvious considerations concerning the surface brightness fluctuation method. Clearly, the fluctuation magnitude will depend both on the particular band used, and on the specific metallicity distribution in each galaxy.

8. Summary and Conclusions

Optical and near-IR CMDs for the Galactic bulge have been presented based on data taken with WFI at the ESO/MPG 2.2m telescope and with SOFI at the ESO NTT, respectively. This dataset has been supplemented by the NICMOS photometry from Paper II, and by public 2MASS data. The near-IR CMD has been statistically decontaminated from the disk stars in the foreground, producing a very clean CMD of the bulge. To ensure great statistical significance also for the upper RGB, the SOFI data have been combined with 2MASS data on a larger field including the SOFI field itself, and the 2MASS CMD has also been statistically decontaminated from the foreground stars.

By combining the best near-IR data in each corresponding luminosity range (2MASS, SOFI, and NICMOS) a luminosity function of the Galactic bulge has been constructed that extends over ~ 15 magnitudes, from a few bright AGB stars above the RGB tip, down to almost the bottom of the main sequence, corresponding to stars of $\sim 0.15 M_{\odot}$. This is the most extended and complete luminosity function so far obtained for the galactic bulge, hence for galactic spheroids in general.

Combining WFI optical data and 2MASS near-IR data, a disk decontaminated ($K, V - K$) CMD was constructed that includes 503 stars brighter than $M_K = -4.5$. Together with empirical RGBs of globular clusters of known metallicity used as templates, this fairly large sample of bulge stars is used to determine the bulge metallicity distribution. It is found to peak at $[\text{M}/\text{H}] \sim -0.1$, with a fairly sharp edge just above solar metallicity, and a low-metallicity tail that does not appreciably extend below $[\text{M}/\text{H}] \sim -1$, quite similar to the spectroscopic result of McWilliam & Rich (1994), but relative to a much larger sample. Such a distribution contains somewhat less metal poor stars than predicted by the *closed box model* of chemical evolution (e.g., Rich 1990), and indicates that the classical *G-dwarf problem* may affect also the Galactic bulge, as known since a long time for the disk (e.g., Tinsley 1980). Integrated light studies indicate that a G-dwarf problem is also present in early type galaxies, as a closed-box model metallicity distribution will result in too low values of the Mg_2 index (Greggio 1997). Yet, the reasons for both disks and spheroids sharing the same problem are likely to be at least in part quite different. For the Galactic disk (and perhaps disks in general) pre-enrichment by the older bulge is likely to set a floor metallicity at $[\text{Fe}/\text{H}] \sim -1.0$ (Renzini

2002). Clearly, this kind of pre-enrichment cannot be invoked for the bulge itself.

In the closed-box model one assumes the whole baryonic mass to be already assembled at $t = 0$, while by adopting a gradual built up the G-dwarf problem can be eliminated. In the case of the Galactic disk this solution of the problem has taken the name of *infall* (e.g. Pagel 1997, and references therein). Since the star-forming ISM (either in a disk or in a proto-spheroid) is likely to be built up gradually, then the closed-box model would not apply. This situation is indeed established both in the case of continuous gas infall forming disks, as well as in the case of early, merging-driven starbursts building galactic spheroids. In turn, starbursts are likely to drive metal-rich galactic winds, thus discontinuing star formation before the gas is fully turned into stars. Therefore, the bulge likely departed from the closed-box approximation both for having being built gradually, albeit rapidly, and for having ejected gas and metals near the climax of its star formation activity.

The near-IR CMD of the Galactic bulge, carefully decontaminated from foreground stars, has been used to show that the bulge is virtually coeval with the Galactic halo. The region in the CMD above the main sequence turnoff of the bulge is so devoid of stars that no trace can be found of a population of bulge stars significantly younger than the main old component. This indicates that no appreciable new stars formed in the bulge, or were added to it, following the intense starburst activity that turned $\sim 10^{10} M_{\odot}$ of gas into the bulge stars, some 10 Gyr ago.

Using both optical and near-IR data, the RGB tip of the bulge is clearly identified, and its systematics in the various bands is established. Contrary to the behavior at lower metallicities, in the metallicity range spanned by the bulge stars ($-1 \lesssim [\text{Fe}/\text{H}] \lesssim 0$) the I -band luminosity of the RGB tip is not constant, but decreases with increasing metallicity. Conversely, the RGB tip luminosity is found to be constant in the H band, while it increases with metallicity in the K band. This behavior is naturally accounted for by a combination of increasing blanketing which is stronger at short wavelengths (i.e. in the I and J band), with the bolometric luminosity of the RGB tip which increases with increasing metallicity. The metallicity distribution of galactic spheroids is therefore expected to affect the use of the surface brightness fluctuation method of distance determinations (Tonry & Schneider 1988). As a final remark, we would like to note that a group of stars is found at luminosities exceeding the RGB tip, and their number is roughly consistent with the expectation scaling from old, metal rich globular clusters. Their number is consistent with the purely old age for the bulge population as derived from the turnoff region.

Worth mentioning are also some limitations of the present study. The location of the peak of the metallicity distribution coincides with the metallicity of the clusters NGC 6528 and NGC 6553, but in turn the metallicity itself of these clusters remain quite uncertain. Systematic,

homogeneous, high spectral resolution studies of stars in these clusters and in the field are needed to properly match the cluster and field star metallicity scales. When such data will become available, it will be easy to re-derive the metallicity distribution of the bulge. Finally, we regret to have been unable to find the origin of the larger HB and RGB spread exhibited by the bulge CMD, compared to simulations that are meant to include all intrinsic spreads of the real bulge population (distance, metallicity, and reddening).

In closing, we would like to note that the Milky Way galaxy is a rather unobscured late-type spiral, member of a poor group of galaxies located quite away from major density peaks in the distribution of galaxies. Yet, virtually its whole spheroidal component, from the outer metal-poor halo all the way to the central metal-rich bulge, is ~ 1 Hubble time old. There is now conclusive evidence that the stellar populations of galactic spheroids in general, elliptical and bulges, are also ~ 1 Hubble time old (e.g. Renzini 1999, for an extensive review), while most such spheroids appear to be well in place and fully assembled already at $z \sim 1$, having passively evolved since at least $z \sim 2.5$ (Cimatti et al. 2002). If the stellar mass in galactic spheroids amounts to 50-70% of the total stellar mass in the local universe (Fukugita et al. 1998), all this evidence indicate that a major fraction of all stars formed at high redshift, in deep potential wells bound to become the galactic spheroids of today. If such build up of galaxies was promoted by the hierarchical merging of dark matter halos, it took place at a time and at a rate that no practical rendition of the hierarchical merging paradigm has yet succeeded to reproduce (Cimatti et al. 2002 and references therein).

Acknowledgements. We thank the referee, Dr. E.M. Sadler, for careful reading of the manuscript and comments that lead to an improvement of the paper.

The present work has been partially supported by the Italian Ministero della Università e della Ricerca under the program “*The Origin and Following Evolution of the Stellar Population in the Galactic Spheroid*” and by the Agenzia Spaziale Italiana.

S.C. acknowledges the financial support by (Cofin2001) under the scientific project: “Origin and evolution of stellar populations in the galactic spheroid”

RMR acknowledges support from grant number AST-0098739, from the National Science Foundation and from grant GO-7891 from the Space Telescope Science Institute.

References

- Allen’s Astrophysical Quantities, 2000, 4th edition, ed. Cox, A.N. (New York: Springer-Verlag)
- Barbuy, B. 1999, *Ap&SS*, 265, 319
- Barbuy, B., Renzini, A., Ortolani, S., Bica, E., & Guarnieri, M.D., 1999, *A&A* 341, 539
- Bono, G., Caputo, F., Cassisi, S., Castellani, V., & Marconi, M. 1997, *ApJ*, 479, 279
- Cardelli, J. A., Clayton, G. C., & Mathis, J. S. 1989, *ApJ*, 345, 245
- Carney, B.W. 1996, *PASP*, 108, 900
- Carretta, E., Cohen, J.G., Gratton, R.G., Behr, B.B. 2001, *AJ*, 122, 1469
- Carpenter, J.M. 2001, *AJ*, 121, 2851
- Cassisi, S., Castellani, V., Ciarcelluti, P., Piotto, G., & Zoccali, M. 2000, *MNRAS*, 315, 679
- Cassisi, S., Salaris, M., & Bono, G. 2002, *ApJ*, 565, 1231
- Cassisi, S., & Salaris, M. 1997, *MNRAS*, 285, 593
- Castelli, F., Gratton, R.G., Kurucz, R.L., 1997, *A&A*, 318, 841
- Cimatti, A., Daddi, E., Mignoli, M., Pozzetti, L., Renzini, A. et al. 2002, *A&A* (in press, astro-ph/0111527)
- Coelho, P., Barbuy, B., Perrin, M.-N., Idiart, T., Schiavon, R.P., Ortolani, S., Bica, E., 2001, *A&A*, 376, 136
- Cohen, J.G., Gratton, R.G., Behr, B., Carretta, E., 1999, *ApJ*, 523, 739
- Cole, A.A., & Weinberg, M.D. 2002, *ApJ*, 574, L43
- Coté, P. 1999, *AJ*, 118, 406
- Davidge, T.J. & Nieto J.-L., 1992, *ApJ*, 391, L13
- Depoy, D.L., Terndrup, D.M., Frogel, J.A., Atwood, B., Blum, R. 1993, *AJ*, 105, 2121
- Elston, R., & Silva, D.R., 1992, *AJ*, 104, 1360
- Faber, S.M., Friel, E.D., Burstein, D., & Gaskell, C.M. 1985, *ApJS*, 57, 711
- Feltzing, S. & Gilmore, G. 2000, *A&A*, 355, 949
- Feltzing, S., Johnson, R.A., & de Cordova, A. 2002, *A&A*, 385, 67
- Ferraro, F., Fusi Pecci, F., & Bellazzini, M. 1995, *A&A*, 294, 80
- Ferraro, F.R., Montegriffo, P., Origlia, L., & Fusi Pecci, F. 2000, *AJ*, 119, 1282
- Forbes, D.A., Brodie, J.P., & Larsen, S. 2001, *ApJ*, 556, L83
- Freedman, W.L., 1992, *AJ*, 104, 1349
- Frogel, J.A., & Elias, J.H. 1988, *ApJ*, 324, 823
- Frogel, J.A., & Whitelock, P.A. 1998, *AJ*, 116, 754
- Frogel, J.A., & Whitford, A.E. 1987, *ApJ*, 320, 199
- Frogel, J.A., Stephens, A., Ramirez, S., DePoy, D.L. 2001, *AJ*, 122, 1896
- Fugugita, M., Hogan, C.J., & Peebles, P.J.E. 1998, *ApJ*, 503, 518
- Greggio, L. 1997, *MNRAS*, 285, 151
- Greggio, L., Tosi, M., Clampin, M., De Marchi, G., Leitherer, C., Nota, A. & Sirianni, M. 1998, *ApJ*, 504, 725
- Guarnieri, M.D., Renzini, A., & Ortolani, S. 1997, *ApJ*, 477, L21
- Guarnieri, M.D., Ortolani, S., Montegriffo, P., Renzini, A., Barbuy, B., Bica, E., Moneti, A.: 1998, *A&A*, 331, 70
- Harris W.E. 1976, *AJ*, 81, 1095
- Harris W.E. 1996, *AJ*, 112, 1487
- Harris W.E. 2001, in *Star Clusters*, ed. L. Labhardt & B. Binggeli (Berlin: Springer-Verlag), p. 223
- Hartwick, F.D.A. 1976, *ApJ*, 209, 418
- Holtzman, J.A., Light, R.M., Baum, W.A., Worthey, G., Faber, S.M., et al. 1993, *AJ*, 106, 1826
- Holtzman, J.A., Watson, A.M., Baum, W.A., Grillmair, C.J., Groth, E.J., et al. 1998, *AJ*, 115, 1946
- Iben, I. Jr. 1968, *ApJ*, 154, 581
- Iben, I. Jr., & Renzini, A. 1983, *ARA&A*, 21, 271
- Kent, S.M. 1992, *ApJ*, 387, 181
- Kinney, A.L., Calzetti, D., Bohlin, R.C., McQuade, K., Sorchil-Bergmann, T., & Schmitt, H.R. 1996, *ApJ*, 467, 38
- Landolt, A.U. 1992, *AJ*, 104, 340
- Lee, M.G., Freedman, W., & Madore, B.F. 1993, *ApJ*, 417, 553
- Mannucci, F., Basile, F., Poggianti, B.M., Cimatti, A., Daddi, E., Pozzetti, L., & Vanzi, L. 2001, *MNRAS*, 326, 745

- Maraston, C., Greggio, L., Renzini, A., Ortolani, S., Saglia, R., Puzia T.H., Kissler-Patig M., 2002, *A&A*, in press, (astro-ph/0209220)
- McNamara, D.H, Madsen, J.B., Barnes, J. & Ericksen, B.F. 2000, *PASP*, 112, 202
- McWilliam, A. & Rich, R.M. 1994, *ApJS*, 91, 749
- Minniti, D. 1995, *AJ*, 109, 1663
- Momany, Y., Vandame, B., Zaggia, S., Mignani, R.P., da Costa, L., et al. 2001, *A&A*, 379, 436
- Montegriffo, P., Ferraro, F.R., Origlia, L. & Fusi Pecci, F. 1998, *MNRAS*, 297, 872
- Mould, J.R. 1984, *PASP*, 96, 773
- Ng, Y.K., & Bertelli, G. 1996, *A&A*, 315, 116
- Oke, J.B., & Gunn, J.E. 1983, *ApJ*, 266, 713
- Origlia, L., Rich, R.M., Castro, S. 2002, *AJ*, 123, 1559
- Ortolani, S., Renzini, A., Gilmozzi, R., Marconi, G., Barbuy, E., Bica, E. & Rich, R.M. 1995, *Nature*, 377, 701 (Paper I)
- Ortolani, S., Barbuy, B., Bica, E., Renzini, A., Zoccali, M. et al. 2001, *A&A*, 376, 878
- Pasquini, L., Avila, G., Allaert, W., Ballester, P., Biereichel, P., et al. 2000, *SPIE*, 4008, 129
- Pagel, B.E.J. 1997, *Nucleosynthesis and Chemical Evolution of Galaxies* (Cambridge University Press), p. 237
- Persic, M. & Salucci, P. 1992, *MNRAS*, 258, 14
- Persson, S.E., Murphy, D.C., Krzemiński, W., Roth, M., Rieke, M.J, 1998, *AJ*, 116, 2475
- Puzia, T.H., Saglia, R.P., Kissler-Patig, M., Maraston, C., Greggio, L., Renzini, A., Ortolani, S. 2002, *A&A* in press (astro-ph/0209238)
- Ramirez, S.V., Stephens, A.W., Frogel, J.A., DePoy, D.L. 2000, *AJ*, 120, 833
- Rejkuba, M., 2002, PhD Thesis (Pontificia Universidad Católica de Chile)
- Renzini, A. 1991, in *Observational Tests of Cosmological Inflation*, ed. T. Shanks, A.J. Banday, & R.S. Ellis (Dordrecht: Kluwer), p. 131
- Renzini, A. 1997, *ApJ*, 488, 35
- Renzini, A. 1998, *AJ*, 115, 2459
- Renzini, A. 1999, in *The Formation of galactic Bulges*, ed. C.M. Carollo, H.C. Ferguson, & R.F.G. Wyse (Cambridge University Press), p. 9
- Renzini, A. 2002, in *Chemical Enrichment of Intracluster and Intergalactic Medium*, ed. F. Matteucci and R. Fusco-Femiano ASP Conf. Ser., 253, 331
- Renzini, A. & Buzzoni, A. 1986 in *Spectral evolution of galaxies*, ed. C. Chiosi & A. Renzini (Dordrecht: Reidel), p. 135
- Rich, R.M. 1988, *AJ*, 95, 828
- Rich, R.M. 1990, in *Bulges of Galaxies*, ed. B.J. Jarvis & D.M. Terndrup (Garching: ESO), p. 65
- Rich, R. M., Ortolani, S., Bica, E., & Barbuy, B. 1998, *AJ*, 116, 1295
- Rich, R.M., Origlia, L., & Castro, S.M. 2001, in preparation
- Rood, R.T., 1972, *ApJ*, 177, 681
- Rosenberg, A., Saviane, I., Piotto, G. & Aparicio, A. 1999, *AJ*, 118, 2306
- Sadler, E.M., Rich, R.M., Terndrup, D.M. 1996, *AJ*, 112, 171
- Sakai, S., Madore, B.F., & Freedman, W. 1999, *ApJ*, 511, 671
- Salaris, M. & Cassisi, S. 1996, *A&A*, 305, 858
- Salaris, M. & Cassisi, S. 1997, *MNRAS*, 289, 406
- Salaris, M. & Cassisi, S. 1998, *MNRAS*, 298, 166
- Salaris, M., Cassisi, S. & Weiss, A. 2002, *PASP*, 114, 375
- Salaris, M. & Weiss, A. 2002, *A&A*, 388, 492
- Saviane, I., Rosenberg, A., Piotto, G., & Aparicio, A. 2000, *A&A*, 355, 966
- Searle, L. & Sargent, W.L.W. 1972, *ApJ*, 173, 25
- Sellwood, J. & Sanders, R., *MNRAS*, 233, 611
- Steidel, C.C., Giavalisco, M., Dickinson, M. & Adelberger, K.L. 1996, *AJ*, 112, 352
- Stephens, A.W., Frogel, J.A., Ortolani, S., Davies, R., Jablonka, P., Renzini, A., & Rich R.M. 2000, *AJ* 119, 419
- Stetson, P.B. 1987, *PASP*, 99, 191
- Stetson, P.B. 1994, *PASP*, 106, 250
- Stetson, P.B. 2000, *PASP*, 112, 925
- Sweigart, A.V., & Gross, P.G. 1978, *ApJS*, 36, 405
- Tantalo, R., Chiosi, C., Bressan, A. & Fagotto, F. 1996, *A&A*, 311, 361
- Terndrup, D.M., 1988, *AJ*, 96, 884
- Tiede, G.P., Frogel, J.A., & Terndrup, D.M. 1995, *AJ*, 110, 2788
- Tinsley, B.M. 1980, *Fund. Cosmic Phys.* 5, 287
- Tonry, J. & Schneider, D.P. 1988, *AJ*, 96, 807
- van Dyk, S. 2000, *BeSN*, 34, 40
- Zinn, R. 1996, *ASP Conf. Ser.* 92, 211
- Zoccali, M., Cassisi, S., Bono, G., Piotto, G., Rich, R.M., & Djorgovski, S.G. 2000, *ApJ*, 538, 289
- Zoccali, M., Cassisi, S., Frogel, J.A., Gould, A., Ortolani, S., Renzini, A., Rich, R.M., Stephens, A.W. 2000, *ApJ*, 530, 418 (Paper II)
- Zoccali, M., Renzini, A., Ortolani, Bica, E., & Barbuy, B. 2001a, *AJ*, 121, 2638
- Zoccali, M., Renzini, A., Ortolani, S., Bragaglia, A., Bohlin, R., Carretta, E., Ferraro, F.R., Gilmozzi, R., Holberg, J.B., Marconi, G., Rich, R.M., & Wesemael, F. 2001b, *ApJ*, 553, 733